J. Mech. Phys. Solids 153 (2021) 104462

Surface instabilities of constrained elastomeric layers subject to electro-static stressing

John W. Hutchinson
School of Engineering and Applied Sciences,
Harvard University, Cambridge, MA, 02138

Abstract: Surface instabilities on the top surface of a soft elastomeric dielectric layer bonded on its bottom to a stiff substrate are investigated for two electro-static conditions: (I) a voltage difference imposed across the top and bottom surfaces of the layer which are both conducting, and (II) a voltage difference imposed across a rigid planar electrode above the layer and the conducting top surface of the layer. In the absence of surface energy, the critical voltage associated with the onset of instability of the planar state is shown to be a surface mode with any wavelength that is short compared to the layer thickness. With no layer pre-stretch and no surface energy, the uniform state in (I) has hydrostatic compression while that of (II) has hydrostatic tension, nevertheless the critical voltage is the same for both problems if the permittivity is the same for both systems. The role of equi-biaxial pre-stretch and surface energy is presented for both problems for neo-Hookean materials and for the Gent generalization. The thrust of the study is the investigation of the post-bifurcation behavior involving nonlinear interactions among the simultaneous surface modes associated with the critical voltage. The post-bifurcation response of Problem I is a crease-like mode with the top surface probing downward towards the lower surface. The opposite occurs for Problem II with the formation of a sharp ridge protruding towards the upper electrode. The bifurcation behavior is highly unstable leading to an extreme sensitivity to small imperfections. The study complements earlier work and highlights unresolved issues.

1. Introduction

Electrostatic actuation of soft elastomeric materials has been extensively studied in the past decade (Lu et al., 2020), and a variety of instability phenomena have been emerged in these studies. Perhaps the most basic instability problem is that of a planar elastomeric sheet free to expand laterally in its plane whose conducting surfaces are subject to a voltage difference (Plante et al., 2006; Suo, 2010; Lu et al., 2016). The attractive force per area between the surfaces is proportional to the square of the voltage and inversely proportional to the square of the layer

thickness. Under an increasing voltage difference the electrical forces squeeze the sheet and simultaneously act to expand it laterally. At a critical voltage the electrical forces overtake the elastic resistance of the sheet and an instability occurs in the form of dynamic snapping to another state of deformation having lower thickness. This type of instability is associated with the attainment of a limit point wherein the sheet remains uniform, thinning and expanding laterally, until a local maximum in the voltage that the sheet can support is attained. For a sheet of incompressible neo-Hookean material that has no pre-stretch and which is free to expand laterally, the local maximum voltage V_0 that can be sustained in the uniform state is (Suo, 2010)

$$\sqrt{\frac{\varepsilon}{\mu}}\frac{|V_0|}{h_0} = 0.687 \tag{1.1}$$

where ε is the permittivity, μ is the ground state shear modulus of the material, h_0 is the thickness of the sheet in the undeformed state, and $h = 0.630\,h_0$ is the thickness at the maximum voltage.

In the course of an investigation of the electro/mechanical stability of coaxial fibers made of elastomeric materials (Clarke and Hutchinson, 2021), it was noticed that there exist limiting situations in which thin layers of elastomers, configured such that they were constrained against lateral expansion, experienced surface instabilities similar in some respects to those Biot (1963, 1965)) analyzed for compressed elastomeric half-spaces. This led to the present study of instability of the two constrained layer problems sketched in Fig. 1. We begin by presenting results in Section 2 from a bifurcation analysis (a linear stability analysis) of the onset of instability of the perfect flat layers showing that multiple critical modes of instability occur simultaneously in the form of wrinkling confined to the surface of the layer. The constraint of the rigid substrate eliminates the possibility of loss of stability at a limit point. An initial post-bifurcation analysis is then performed in the subsequent sections which demonstrates that the nonlinear interaction among the simultaneous wrinkling modes is associated with highly unstable surface wrinkling and a critical voltage with an exceptionally strong sensitivity to small imperfections. The post-bifurcation analysis indicates that the wrinkles in Problem I combine to form a crease-like entity while those in Problem II combine to form a ridge. Experimental observations by Kofod et al. (2003) and Wang et al. (2011a) of constrained elastomer layers with

the configuration of Problem I in Fig. 1 have revealed an abrupt occurrence of crease-like surface modes and, moreover, that the voltage at which these surface instabilities occur can be significantly influenced by pre-stretching the layer before it is bonded to the stiff substrate.

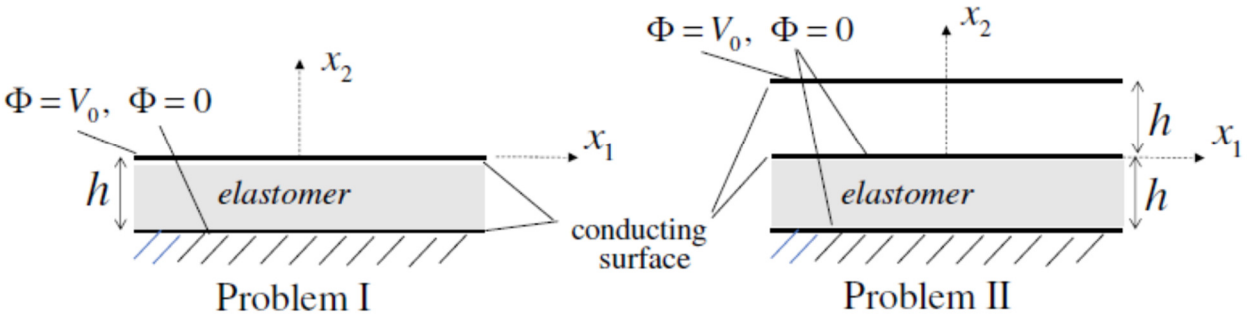

Fig. 1 The two constrained layer problems in the uniform state. Prior to bonding to the rigid substrate, the layers are subject to an equi-biaxial pre-stretch λ_0. Plane strain instability modes are analyzed.

Wang et al. (2011a) and Park et al. (2013) carried out numerical (finite element) studies discussed later in this paper of Problem I focused on finding the lowest voltage at which crease-like surface instabilities can exist. These authors bypassed the classical bifurcation analysis of linear stability of the perfectly flat layer and instead sought the lowest voltage at which finite strain, crease-like solutions have the same system energy as the perfectly flat layer. When Wang et al. (2011a) conducted their groundbreaking experiments and numerical work, they drew on theoretical advances that had only recently been achieved in the understanding of surface wrinkling and creasing of compressed elastomeric half-spaces. Decades after Biot (1963) analyzed short wavelength surface wrinkling instabilities via a bifurcation (linear stability) analysis, Hohlfeld and Mahadevan (2008, 2001) showed that finite strain, creasing solutions with arbitrarily small size exist at lower compressive strains than the strains predicted by Biot's bifurcation analysis of surface wrinkling. This finding finally explained (Wei et al., 2009) the long-standing experimental observations of creases, and not wrinkles, at the surface of compressed elastomers (Tanaka et al., 1987).

To our knowledge, the bifurcation (linear stability) analyses of the electro-mechanical stability of Problems I and II presented in Section 2 have not been previously appeared in the literature Even though the critical voltage from the bifurcation analysis will almost certainly be

an upper bound to observations of surface wrinkling or creasing, this analysis is traditionally the first step in any stability investigation of an elastic system, and it informs trends dependent on pre-stretch and surface energy. The bifurcation results have the added attraction in the present instance that they are exact and expressed as simple formulas. Moreover, these classical stability analyses provide clear insights as to what does and does not drive the instability. For example, it is not the compressive stresses induced by the electric field that drive the instabilities of interest here. This will be evident from the fact that in the absence of pre-stretch the two problems in Fig. 1 have the same critical voltage if the permittivity is the same in each system even though one layer is in a state of hydrostatic compression and the other in hydrostatic tension. The body of the paper in Sections 3-5 presents an investigation of the nonlinear initial post-bifurcation behavior of the wrinkling mode, revealing that the simultaneous surface wrinkling modes combine to form crease-like or ridge-like mode shapes. Imperfection-sensitivity of the maximum attainable voltage is also analyzed. Comparisons in Section 6 of the present results with experimental and numerical results in the literature for Problem I on crease formation expose some open issues remaining to be resolved when pre-stretch is present. The arrangement of the conducting surfaces leading to an upward traction on the elastomer top surface and a hydrostatic tension in the pre-bifurcation state, has featured prominently in experimental studies of thin viscous fluid layers (see the review by Wu and Russel (2009)) revealing an intriguing variety of instability patterns formed on the layer surface including periodic arrays of pillar and ridge-like entities rather than creases. Problem II produces upward traction and hydrostatic tension on the elastomer layer and generates ridge-like modes, but it does not model all aspects present in some of the experimental arrangements.

2. Onset of instability in electro-statically loaded constrained elastomeric layers

The elastomeric layers in the two configurations in Fig. 1 are taken to be an incompressible, neo-Hookean solid with shear modulus μ, although Gent's (1996) extension of the neo-Hookean model will also be considered in Section 6. Prior to bonding the bottom of the layer to a rigid substrate the layer is subject to an equi-biaxial pre-stretch, λ_0, in the plane of (x_1, x_3). In the uniform, pre-stretched state the layer thickness is h with the bottom surface at $x_2 = -h$ and the top surface at $x_2 = 0$. The elastomer is idealized to be non-conducting with

permittivity ε whose surfaces have been functionalized to be conducting. A surface energy per area, γ, of the elastomer top surface will be considered. In Problem I, a voltage difference V_0 is imposed across the top and bottom surfaces of the layer as shown in Fig. 1. In Problem II, V_0 is imposed across a rigid planar electrode held at $x_2 = h$ and the top surface of the layer, and there is no voltage difference across the top and bottom surfaces of the elastomer. The permittivity is denoted by ε, which generally will differ in value for the two problems.

In Problem I there is electro-static attraction between the top and bottom surfaces of the elastomer which, prior to any instability, produces a uniform traction (force per area) $T_2 = -\varepsilon(V_0/h)^2/2$ acting on the top surface. Because the layer is incompressible and constrained against lateral motion along its bottom surface, the electro-static attraction generates a state of hydrostatic compression superimposed on the pre-stress in the layer such that the stresses are $\sigma_{22} = -\varepsilon(V_0/h)^2/2$ and $\sigma_{11} = \sigma_{33} = \mu(\lambda_0^{\,2} - \lambda_0^{\,-4}) - \varepsilon(V_0/h)^2/2$, with stretches $\lambda_1 = \lambda_3 = \lambda_0$, $\lambda_2 = \lambda_0^{\,-2}$. In Problem II, the electro-static attraction produces an upward traction on the top surface of the elastomeric layer such that the stresses are $\sigma_{22} = \varepsilon(V_0/h)^2/2$, $\sigma_{11} = \sigma_{33} = \mu(\lambda_0^{\,2} - \lambda_0^{\,-4}) + \varepsilon(V_0/h)^2/2$ with stretches $\lambda_1 = \lambda_3 = \lambda_0$, $\lambda_2 = \lambda_0^{\,-2}$. In the absence of pre-stretch, the pre-bifurcation state of Problem I is hydrostatic compression while Problem II is in a state of hydrostatic tension.

We have investigated bifurcation from the perfectly planar state in the form of plane strain, periodic instability modes having wavelength, $\ell = 2\pi/k$, in the x_1 direction with k as the wavenumber. The bifurcation analysis (linear stability analysis) is given in the Supporting Materials. The dimensionless voltage parameter characterizing the onset of instability is $\Omega = (\varepsilon/\mu)(V_0/h)^2$ or the square root thereof, $\sqrt{\Omega} = \sqrt{\varepsilon/\mu}\,|V_0|/h$. The result of the bifurcation analysis for the case of no pre-stretch and no surface energy is the eigenvalue spectrum plotted in Fig. 2. The features of primary interest to the present study are the fact that the critical (lowest) eigenvalue is the short-wavelength limit and that Ω_C for this limit is the same for Problem I and II. Moreover, at $\ell/h = 1$ the eigenvalue is less than 0.1% above the short-wavelength limit and

thus this limit is in play for all wavelengths below $\ell \cong h$. The critical limiting eigenvalue for wrinkling is

$$\Omega_C = 4(\sqrt{2}-1) = 1.657 \quad \text{or} \quad \sqrt{\Omega_C} = \sqrt{\varepsilon/\mu}\,|V_0/h| = 1.287 \qquad \text{(Problems I \& II)} \qquad (2.1)$$

and the associated eigenmodes (for any $kh > 2\pi$) are

$$u_1 = -\left(1+b(1+kx_2)\right)e^{kx_2}\sin kx_1\,,\; u_2 = \left(1+bkx_2\right)e^{kx_2}\cos kx_1 \qquad (2.2)$$

with $b = -\sqrt{2}$ for Problem I and $b = -\left(2-\sqrt{2}\right)$ for Problem II. These are surface modes which decay exponentially below the surface and do not interact with the bottom of the elastomer layer. The length h enters the criticality condition (2.1) because the electric field is set by h.

Although these linear stability results and those to follow do not seem to have been previously reported, a relevant and insightful early analysis of a version of Problem I was given by Huang (2005). That analysis used linear elasticity to model the layer which introduces an approximation even though the strains at bifurcation are zero because the hydrostatic stresses are on the order of the elastic shear modulus. Nevertheless, Huang's result, which is $\sqrt{\Omega_C} = \sqrt{2}$ in our notation, only exceeds the correct result by 10%.

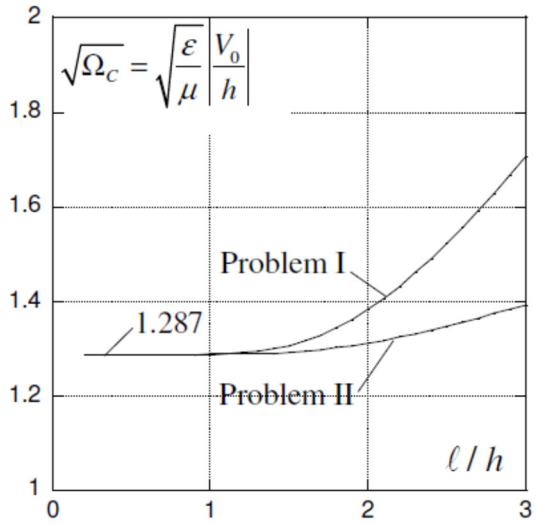

Fig. 2 The bifurcation eigenvalue spectrum for the two neo-Hookean layer problems with no pre-stretch ($\lambda_0 = 1$) and no surface energy ($\gamma = 0$). The short wavelength limit is attained when ℓ / h is less than about unity.

The fact that Problems I and II have the same dimensionless critical voltage, even though (I) is in a state of hydrostatic compression and (II) has hydrostatic tension, illustrates that it is not compressive stress that is driving the instability in (I). Compressive stresses do not necessarily lead to instability as illustrated by the fact that a neo-Hookean layer bonded to a rigid substate and subject to a hydrostatic fluid pressure on its top surface is stable at all pressures. Instead, the instability in Problems I and II is driven by the strong coupling between the changes in the electrostatic forces arising from undulations of the top surface and the corresponding elastic deformation. Given the central role of the critical voltage predicted by the bifurcation analysis, we have included the functional on which the bifurcation analyses in this paper are based in Section 4. It reveals the strong coupling referred to above and includes the effect of equi-biaxial pre-stretch, λ_0, and surface tension, γ, and it employs the Gent generalization of the neo-Hookean model which includes one extra material parameter, J_L, described in Section 6.

The effect of surface energy is seen in Fig. 3. The influence is greatest at the shortest wavelengths such that the lowest value of the voltage for the onset of the instability is no longer the limit for $\ell / h \to 0$ but instead depends on γ. For the experimental system of PDMS layers (Wang et al., 2011a) discussed in Section 6, representative values of the parameters are $h = 40 - 200\mu m$, $\mu = 10 - 200kPa$ and $\gamma = 0.04 Jm^{-2}$ corresponding to $0.001 < \gamma / \mu h < 0.1$. At the lowest values of this range, surface energy has almost no effect on the critical onset of the instability but would limit the critical wavelengths to lie in the range from about $h/4$ to h. At the high end of the range, $\gamma / \mu h \approx 0.1$, the surface energy raises the critical voltage significantly and limits the range of the critical wavelengths even more. A study by Wang et al. (2013) presents experiments on electro-static surface instabilities of constrained layers over a wide range of $\gamma / \mu h$ revealing a transition from creasing to wrinkling when $\gamma / \mu h > 1$.

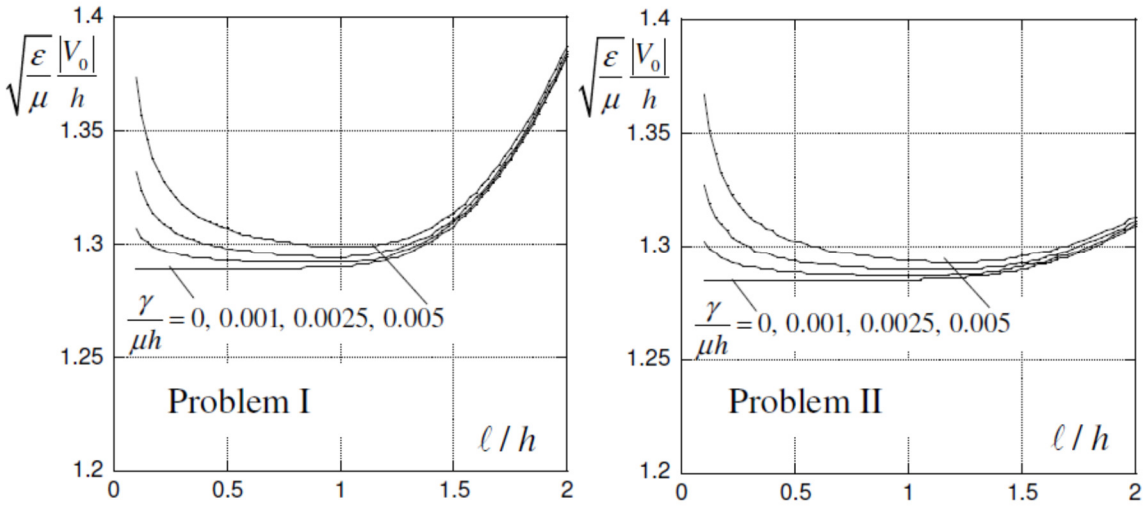

Fig. 3 The effect of surface energy on the bifurcation eigenvalue spectrum for the layer problems for the case of neo-Hookean materials with no pre-stretch ($\lambda_0 = 1$).

Two figures will be used to show the effect of pre-stretch λ_0 on the onset of instability, the first, Fig. 4, presenting the voltage eigenvalue spectrum as a function of wavelength with no surface energy, and the second showing only the critical (lowest) voltage, including the influence of surface energy, to follow later. Fig. 4 reveals that pre-stretch affects Problems I and II differently. For Problem I, pre-stretch increases the critical voltage, while for Problem II, pre-stretch in the range $1 < \lambda_0 < 2$ lowers the critical voltage. Above $\lambda_0 = 2$, pre-stretch increases the critical voltage for Problem II but not as much as for Problem I, as will be seen shortly. It remains true that the lowest voltage eigenvalue with pre-stretch and no surface energy occurs in the short wavelength limit. It can also be seen that pre-stretch increases the range of the short wavelength limit to values of ℓ / h well above unity.

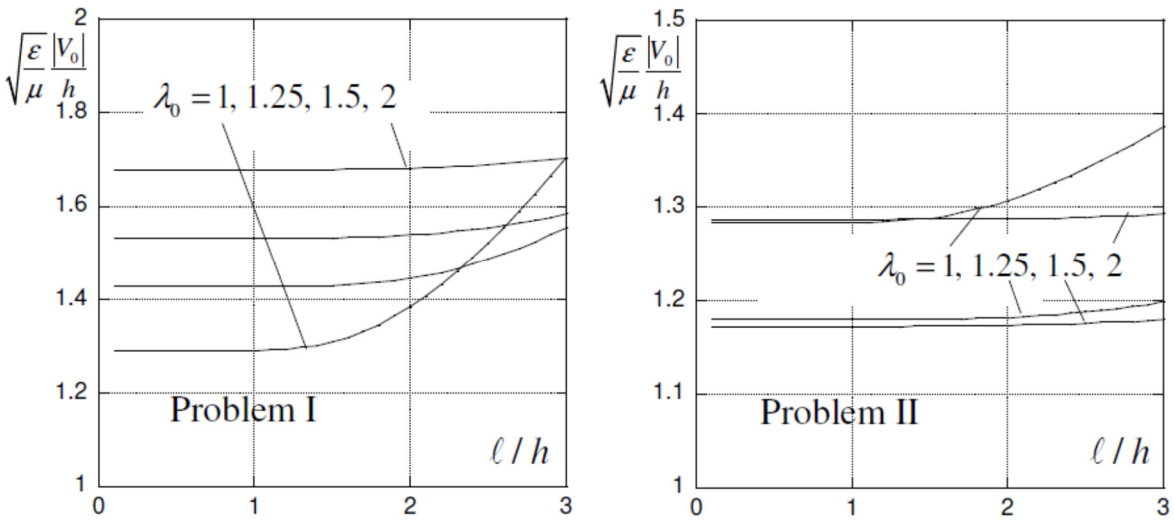

Fig. 4 The effect of equi-biaxial pre-stretch λ_0 on the voltage eigenvalue spectrum for the two layer problems for neo-Hookean materials in the absence of surface energy ($\gamma = 0$).

2.1 The short wavelength limit for sinusoidal surface instabilities

From Figs. 3 and 4 it can been inferred that the critical (lowest) bifurcation mode is a short wavelength surface mode which does not interact with the clamped bottom of the layer as long as the dimensionless surface energy $\gamma / \mu h$ is less than about 0.005. The thickness of the layer h sets the voltage gradient V_0 / h imposed on the surface, but otherwise does not play a role in the instability. In the short wavelength limit the only length quantity in the problem is the wavelength itself, $\ell = 2\pi / k$. Denote the unperturbed electric field imposed on the layer surface by $\mathbf{E} = V_0' \mathbf{i}_2$ where the voltage gradient is $V_0' = V_0 / h$. In the Support Materials, we have formulated and analytically solved the short wavelength bifurcation problem for the critical voltage gradient and associated modes at the onset of the surface instability. Equations (2.1) and (2.2) provide the critical voltage measured by $\Omega_C = \varepsilon V_0'^2 / \mu$ and the associated simultaneous linear stability modes when there is no pre stretch and no surface energy. The results for the critical voltage that account for pre-stretch and surface energy are

$$\Omega_C = 2\lambda_0^{-2}\sqrt{\left(\lambda_0^{3}+1\right)\left(\lambda_0^{2}+3\lambda_0^{-4}+2\pi\gamma/\mu\ell\right)}-4\lambda_0^{-4} \quad \text{(Problem I)} \qquad (2.3)$$

$$\Omega_C = 2\lambda_0^{-4}\sqrt{\left(\lambda_0^{\,3}+1\right)\left(\lambda_0^{\,6}+4\lambda_0^{\,3}-1+(2\pi\gamma/\mu\ell)\lambda_0^{\,4}\right)}-4\lambda_0^{-1} \quad \text{(Problem II)} \tag{2.4}$$

with the modes presented later. The dimensionless surface energy parameter is taken as $\gamma/\mu\ell$ in the surface instability analysis. For small pre-stretch, i.e., $\lambda_0 = 1+\Delta\lambda_0$ with $\Delta\lambda_0$ not larger than about 0.2, and surface energy not larger than about $\gamma/\mu\ell \cong 0.1$, the following lowest order expansions of (2.3) and (2.4) in $\Delta\lambda_0$ and $\gamma/\mu\ell$ are reasonably accurate:

$$\Omega_C = 4(\sqrt{2}-1)+2(8-5\sqrt{2})\Delta\lambda_0+\sqrt{2}\pi\gamma/\mu\ell \qquad \text{(Problem I)} \tag{2.5}$$

$$\Omega_C = 4(\sqrt{2}-1)(1-\Delta\lambda_0)+\sqrt{2}\pi\gamma/\mu\ell \qquad \text{(Problem II)} \tag{2.6}$$

Equations (2.3) and (2.4) are plotted as $\sqrt{\Omega_C}$ in Fig. 5 for pre-stretches $1 \le \lambda_0 \le 5$. The strongest sensitivity to pre-stretch occurs for relatively small pre-stretches. At larger pre-stretch the influence of surface energy is reduced due to the increase in incremental stiffness of the pre-stretched material. The results at appreciable pre-stretch in Fig. 5 will differ for other elastic constitutive models as discussed in detail in Section 6.

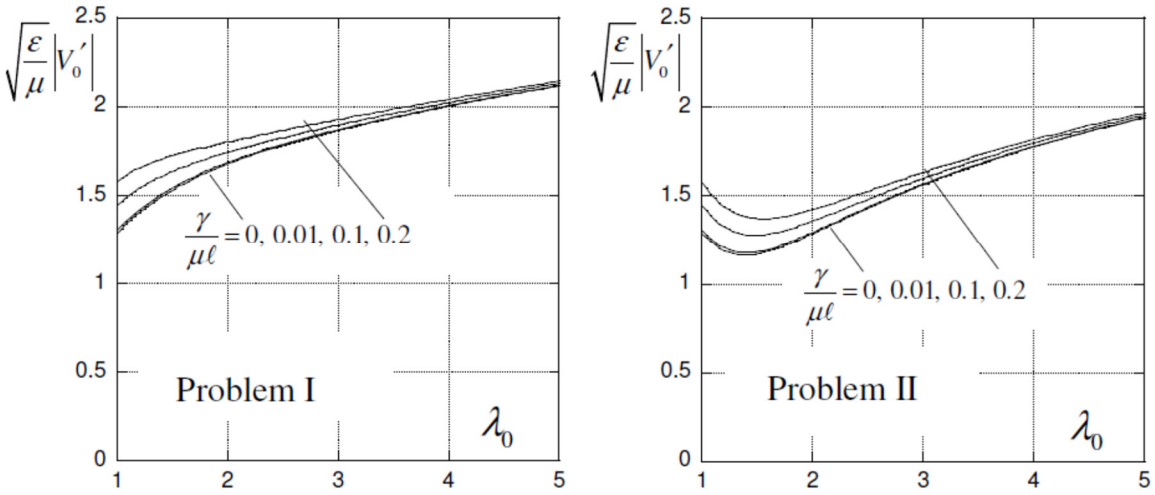

Fig. 5 The critical voltage for sinusoidal surface instabilities for the two layer problems as dependent on equi-biaxial pre-stretch λ_0 and surface energy parameter $\gamma/\mu\ell$ where ℓ is the mode wavelength. These are results of the short wavelength analysis for the neo-Hookean material and only apply if the mode wavelength ℓ is less than about the layer thickness h.

The results discussed thus far and in the remainder of the paper are for plane strain instabilities. However, because the pre-bifurcation state in the current problems is equi-biaxial, the critical voltage eigenvalue is associated with plane strain modes oriented in any direction in the plane of the layer. Superposition of these plane strain modes can give rise to hexagonal, checkerboard, triangular and even axisymmetric pit or pillar modes all associated with the same critical voltage. The post-bifurcation behavior of these other modes will not be investigated here.

The body of this paper is devoted to studying the nonlinear interaction among short-wavelength modes that become critical simultaneously at the same applied voltage. Specifically, the coupling of plane strain modes of with period ℓ in the x_1 direction is investigated using the initial post-bifurcation method originated by Koiter (1945)—see also the book on Koiter's theory by van der Heijden (2009). It will be shown that the nonlinear interaction among the bifurcation modes is exceedingly strong implying that the post-bifurcation behavior is highly unstable. Concomitantly, the maximum voltage that can be imposed on the system is extremely sensitively to initial imperfections in the system. The approach of the present study has much in common with the investigation of the stability of Biot surface wrinkling of a compressed neo-Hookean half-space carried out by Cao and Hutchinson (2012). However, unlike the Biot problem, the pre-bifurcation state in the present layer problems (in the absence of pre-stretch) is a pure hydrostatic compression or tension and, as remarked earlier, the primary driving force for the instability in the present problems is the strong geometry dependence of the electro-static forces. As noted in the Introduction, while the relation between surface creasing and Biot surface wrinkling took decades to be understood, the physical importance of electrostatically driven surface creasing was appreciated from the start in the seminal work of Wang et al. (2011a, 2011b, 2013). Consequently, almost no attention seems to have been paid to electrostatically driven surface wrinkling itself or its connection with surface creasing in Problem I or ridging in Problem II. This paper attempts to fill some of those gaps and, in doing so, reveals aspects of the problems which are not yet well characterized.

To make the paper readable and assessable to as broad an audience as possible, the body of the paper presents the essential elements of the analysis with many details of the derivations consigned to the Supporting Materials. The energy functional characterizing the system is laid

out in Section 3, followed by the application of Koiter's post-bifurcation method in Section 4, including accounting for initial imperfections. The results of the analysis are presented and discussed in Section 5 and a comparison with experimental results and numerical simulations of creasing from the literature is made in Section 6.

3. The energy functional for the constrained layer problems in the short wavelength limit

This section is divided into three sub-sections: the elastic energy contribution, the electro-static energy contribution, and the coupled energy functional for the system. Pre-stretch is included but surface energy is assumed to be absent.

3.1 The elastic energy change for deformations of period ℓ

Layers with either no pre-stretch ($\lambda_0 = 1$) or equi-biaxial pre-stretch ($\lambda_1 = \lambda_3 = \lambda_0$, $\lambda_2 = \lambda_0^{-2}$) will be considered . The upper surface of the layer in the pre-stretched, pre-bifurcation state coincides with the plane $x_2 = 0$. A Lagrangian description is used to denote the horizontal and vertical displacements of material points at (x_1, x_2) in the pre-stretched, pre-bifurcation state as $\left(u_1(x_1, x_2), u_2(x_1, x_2)\right)$. The displacements u_i vanish for $x_2 << -\ell$ and are assumed to be periodic in the x_1-direction with period ℓ. Attention will also be restricted to deformations that are symmetric about $x_1 = 0$.

The incompressible neo-Hookean material with ground state shear modulus μ has an energy density written in terms of the principal stretches, $(\lambda_I, \lambda_{II}, \lambda_{III})$, as

$$W = \frac{1}{2}\mu\left(\lambda_I^{\,2} + \lambda_{II}^{\,2} + \lambda_{II}^{\,2} - 3\right) \tag{3.1}$$

subject to the incompressibility constraint $\lambda_I \lambda_{II} \lambda_{II} = 1$. For principal stretches parallel to the x_i axes with μq as the Lagrangian multiplier to enforce incompressibility, the true Cauchy stresses are given by

$$\sigma_{11} = \mu(\lambda_1^{\,2} - q),\ \sigma_{22} = \mu(\lambda_2^{\,2} - q),\ \ \sigma_{33} = \mu(\lambda_3^{\,2} - q) \tag{3.2}$$

For the layer problems in Fig. 1, the pre-bifurcation stress state is the hydrostatic compression or tension generated by the electrostatic forces, $\sigma = -\tau\mu\Omega/2$ (with $\Omega = \varepsilon V_0'^2/\mu$, $\tau = 1$ for Problem I, and $\tau = -1$ for Problem II) superimposed on the pre-stretch stresses. Thus, in the pre-bifurcation state $q^0 = (\lambda_0^{-4} + \tau\Omega/2)$ and

$$\sigma_{11}^0 = \sigma_{33}^0 = \mu(\lambda_0^2 - \lambda_0^{-4} - \tau\Omega/2) \quad \text{and} \quad \sigma_{22}^0 = -\mu\tau\Omega/2 \tag{3.3}$$

To represent the elastic energy in a bifurcated state, let $q = q^0 + \Delta q$ where Δq has the same periodicity as the displacements. Then the functional characterizing the elastic energy change from the pre-bifurcation state per unit length in the x_3 direction in a section of one period can be expressed as

$$\begin{aligned}\Delta U^{elastic} = \mu\int_{-\infty}^{0}\int_{-\ell/2}^{\ell/2}\Big\{&\tfrac{1}{2}\lambda_0^2\left(u_{1,1}^2 + u_{2,1}^2\right) + \tfrac{1}{2}\lambda_0^{-4}\left(u_{1,2}^2 + u_{2,2}^2\right)\\ &-\left(\lambda_0^{-4} + \tfrac{1}{2}\tau\Omega\right)\left(u_{1,1}u_{2,2} - u_{1,2}u_{2,1}\right) - \Delta q\left(u_{1,1} + u_{2,2} + u_{1,1}u_{2,2} - u_{1,2}u_{2,1}\right)\Big\}dx_1dx_2\end{aligned} \tag{3.4}$$

where incompressibility of the bifurcated solution requires $u_{1,1} + u_{2,2} + u_{1,1}u_{2,2} - u_{1,2}u_{2,1} = 0$, and exponential decay of the displacements below the surface has been anticipated.

3.2 The electro-static energy changes for deformations of period ℓ

In this subsection we present an expression for the change in electrostatic energy due to a periodic shape change of the upper conducting surface of the layer. The wavelength of the shape change is short compared to the thickness of the elastomer layer so that the thickness plays no role other than to set the unperturbed voltage gradient $V_0' = V_0/h$ at the surface, as previously discussed. The shape change in Fig. 6 is assumed be independent of the out-of-plane coordinate x_3 and symmetric about $x_2 = 0$, and therefore consistent with the plane strain deformations considered in developing the elastic energy functional. Prior to any deformation, the upper surface coincides with the plane $x_2 = 0$, and thus incompressibility of the elastomer requires $\int_{-\ell/2}^{\ell/2} Y(x_1)dx_1 = 0$, with $Y(x_1)$ as the vertical displacement of the upper surface at x_1.

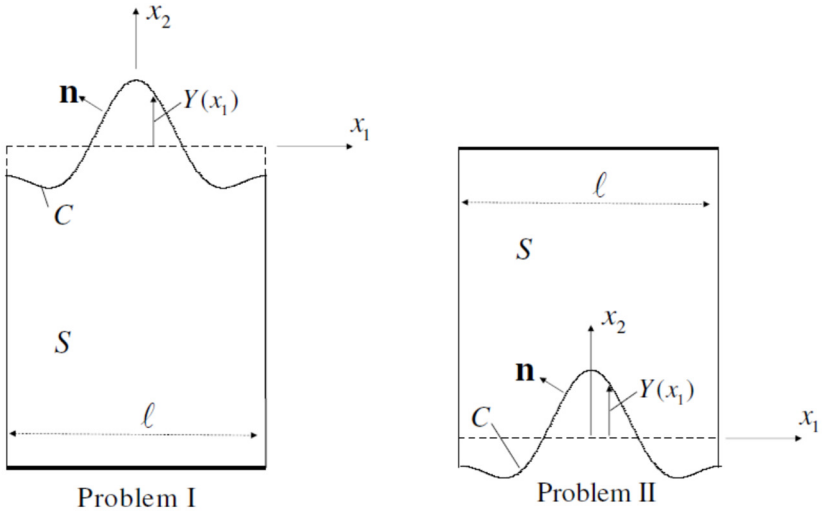

Fig. 6 Periodic sector S in which the energy of the electric field is determined showing the periodic shape change of the top surface C of the elastomeric layer.

Consider Problem I first and denote the voltage potential in the elastomer by $\Phi(x_1, x_2)$ with the electric field as $\mathbf{E} = \vec{\nabla}\Phi$. Prior to any deflection of the surface the electric field is uniform, $\mathbf{E} = V_0'\mathbf{i}_2$, associated with the potential $\Phi = V_0 + V_0' x_2$. If $\ell << h$ ($\ell < h$ will suffice as previously noted) $\Phi \to V_0 + V_0' x_2$ for $x_2 << -\ell$. The potential on the top conducting surface (denoted by C) is held at $\Phi = V_0$. For any surface shape $Y(x_1)$, the potential must satisfy $\nabla^2\Phi = 0$ within S and $\Phi = V_0$ on C. The change in the electric field due to the shape change depends linearly on V_0'. Denote the change in potential due to the shape change $Y(x_1)$ by $V_0'\varphi(x_1, x_2)$ such that $\Phi = V_0 + V_0'(x_2 + \varphi)$ with $\varphi = -Y(x_1)$ on C. The electrical field energy in S per unit length in the x_3 direction is

$$U^{electric} = \frac{1}{2}\varepsilon\int_S \mathbf{E}\bullet\mathbf{E}dS = \frac{1}{2}\varepsilon V_0'^2\int_S \left(1 + 2\varphi_{,2} + \varphi_{,i}\varphi_{,i}\right)dS \tag{3.5}$$

The change of field energy due to the shape change

$$\Delta U^{electric} = \frac{1}{2}\varepsilon V_0'^2\int_S \left(2\varphi_{,y} + \varphi_{,i}\varphi_{,i}\right)dS \tag{3.6}$$

where all the contributions in the integrand decay exponentially below the surface with distance proportional to ℓ.

With

$$Y(x_1)=\sum_{j=1}^{\infty}Y_j\cos jkx_1 \text{ and } Y_j=\frac{2}{\ell}\int_{-\ell/2}^{\ell/2}Y(x_1)\cos jkx_1dx_1,\ j=1,\infty,$$

φ is given by

$$\varphi(x_1,x_2)=\sum_{j=0}^{\infty}\varphi_j e^{jkx_2}\cos(jkx_1) \quad \text{with} \quad \sum_{j=0}^{\infty}\varphi_j e^{jkY(x_1)}\cos(jkx_1)=-Y(x_1) \tag{3.7}$$

To order Y^3 (which is the accuracy required in the present analysis),

$$\Delta U^{electric}=\frac{1}{2}\varepsilon V_0'^2\left\{\pi\sum_{j=1}^{\infty}jY_j{}^2+\frac{\pi^2}{\ell}\sum_{j=1}^{\infty}\sum_{p=1}^{\infty}\sum_{m=1}^{\infty}M_{jpm}Y_jY_pY_m\right\} \text{ (Problem I)} \tag{3.8}$$

where

$$M_{jpm}=\left((j^2-jp-2pm)\left(\beta(p,j+m)+\beta(m,j+p)\right)+(j^2-jp+2pm)\beta(j,m+p)\right) \tag{3.9}$$

with $\beta(i,j)=0$ if $i\neq j$ and $\beta(i,j)=1$ if $i=j$ (see Supporting Materials for details).

The result for Problem II is the same as (3.8) except for a change in sign of the cubic terms (i.e., $+\pi^2/\ell$ is replaced by $-\pi^2/\ell$ in (3.8)).

3.3 The energy functional for the elastomeric layer system subject to a prescribed voltage

When the voltage difference across the two conducting surfaces is fixed at V_0, the change in potential energy of the electro-static forces acting on the top surface of the elastomeric layer from the pre-bifurcation state is $-\Delta U^{electric}$, where we continue to consider a single periodic sector with unit thickness in the x_3 direction. Under prescribed voltage, the energy change of the system (the change in free energy) from the pre-bifurcation state is

$$\Delta\Psi=\Delta U^{elastic}-\Delta U^{electric} \tag{3.10}$$

There remains one difficulty before one can investigate solutions that render $\Delta\Psi$ stationary with respect to the Lagrangian displacement variables $u_1(x_1, x_2)$ and $u_2(x_1, x_2)$. The electrical energy is expressed in terms of the shape of the top surface in the current state $Y(x_1)$ which is related to the Lagrangian displacements by $Y(x_1) = u_2(\overline{x}_1, 0)$ where $x_1 = \overline{x}_1 + u_1(\overline{x}_1, 0)$. To order u_i^2, this connection can be expressed as $Y(x_1) = u_2(x_1, 0) - u_1(x_1, 0)\, u_{2,1}(x_1, 0)$, or with surface displacements denoted by $u(x_1) = u_1(x_1, 0)$ and $v(x_1) = u_2(x_1, 0)$, as

$$Y(x_1) = v(x_1) - u(x_1)v'(x_1) \tag{3.11}$$

with the prime denoting the derivative with respect to x_1.

For the order of accuracy required in the present analysis ($\Delta\Psi$ to order u_i^3) the Fourier coefficients Y_j in the cubic terms in (3.8) can be replaced by the corresponding Fourier coefficients of $v(x_1)$ with errors of order u_i^4, which are being neglected. However, nonnegligible contributions arise from the quadratic terms in (3.8), and it is necessary to account for the second order term in (3.11). To order u_i^3,

$$\sum_{j=1}^{\infty} jY_j^2 = \sum_{j=1}^{\infty} jv_j^2 + \frac{\pi}{\ell}\sum_{j=1}^{\infty}\sum_{p=1}^{\infty}\sum_{m=1}^{\infty} N_{jpm} v_j v_n u_m \tag{3.12}$$

where

$$N_{jpm} = 2jp\left(\beta(m, j+p) + \beta(p, j+m) - \beta(j, m+p)\right)$$

and

$$u_j = (2/\ell)\int_{-\ell/2}^{\ell/2} u(x_1)\sin(jkx_1)dx_1\,, \quad v_j = (2/\ell)\int_{-\ell/2}^{\ell/2} v(x_1)\cos(jkx_1)dx_1 \tag{3.13}$$

The final expression for the energy change of the electric field in terms of the Lagrangian displacement variables and evaluated to order u_i^3 is

$$\Delta U^{electric} = \frac{\pi}{2}\varepsilon V_0'^2 \left\{ \sum_{j=1}^{\infty} j v_j^{\,2} + \frac{\pi}{\ell} \sum_{j=1}^{\infty}\sum_{p=1}^{\infty}\sum_{m=1}^{\infty} \left(\tau M_{jpm} v_j v_p v_m + N_{jpm} v_j v_p u_m \right) \right\} \tag{3.14}$$

where $\tau = 1$ for Problem I and $\tau = -1$ for Problem II.

4. The initial post-bifurcation analysis including the effect of small imperfections

For the periodic surface instability, the only length quantity is the wavelength of the period, $\ell = 2\pi / k$. The voltage parameter V_0' is the uniform electric field imposed on each of the systems in Problems I and II.

In this section, dimensionless variables will be employed consistently. The dimensionless coordinates are $(x, y) = (kx_1, kx_2)$, and the dimensionless displacements are taken to be the dimensional ones divided by ℓ, i.e., $(u_1 / \ell, u_2 / \ell)$ becomes (u_1, u_2) in this section. The dimensionless free energy for one periodic section per unit length in the x_3 direction is

$$\begin{aligned} \frac{\Delta\Psi}{\mu\ell^2} = \int_{-\infty}^{0}\int_{-\pi}^{\pi} \Big\{ & \tfrac{1}{2}\lambda_0^{\,2}\left(u_{1,x}^{\,2} + u_{2,x}^{\,2}\right) + \tfrac{1}{2}\lambda_0^{-4}\left(u_{1,y}^{\,2} + u_{2,y}^{\,2}\right) \\ & -\left(\lambda_0^{-4} + \tfrac{1}{2}\tau\Omega\right)\left(u_{1,x}u_{2,y} - u_{1,y}u_{2,x}\right) - \Delta q\left((u_{1,x} + u_{2,y})/2\pi + u_{1,x}u_{2,y} - u_{1,y}u_{2,x}\right)\Big\} dxdy \\ & -\frac{\pi}{2}\Omega\left\{ \sum_{j=1}^{\infty} j v_j^{\,2} + \pi \sum_{j=1}^{\infty}\sum_{p=1}^{\infty}\sum_{m=1}^{\infty}\left(\tau M_{jpm} v_j v_p v_m + N_{jpm} v_j v_p u_m\right)\right\} \end{aligned} \tag{4.1}$$

with $\tau = 1$ for Problem I and $\tau = -1$ for Problem II. The pre-stretch is λ_0; surface energy is not included.

The bifurcation problem for the critical eigenvalue and associated eigenmodes is governed by the quadratic terms in displacements in the energy functional (4.1) which are denoted by $\Delta\Psi_2$. For all values of the voltage parameter Ω less than the critical eigenvalue, Ω_C, $\Delta\Psi_2 > 0$ for all non-vanishing admissible displacements. The critical eigenvalue is the lowest value of Ω for which $\Delta\Psi_2 = 0$ for some non-vanishing admissible displacements which, when normalized, are the eigenmodes. As discussed in Section 2.1, both Problem I and II have the same critical eigenvalue, $\Omega_C = 4(\sqrt{2} - 1)$, in the absence of pre-stretch. With pre-stretch, Ω_C

is given by (2.3) or (2.4) and plotted in Fig. 5. The associated short wavelength bifurcation mode in the absence of pre-stretch is given by (2.2) while the mode in the presence of pre-stretch is derived in the Support Materials and presented below. The combination of simultaneous eigenmodes in the present analysis having period ℓ (2π in dimensionless coordinates) is

$$u_1 = \sum_{j=1}^{N} \xi_j U^{(j)}(y) \sin jx,\ u_2 = \sum_{j=1}^{N} \xi_j V^{(j)}(y) \cos jx,\ \Delta q = \sum_{j=1}^{N} \xi_j Q^{(j)}(y) \cos jx, \tag{4.2}$$

where ξ_j is the amplitude of the j^{th} mode. The modal functions will be normalized such that $V^{(j)}(0) = 1$ for all j. In the absence of pre-stretch ($\lambda_0 = 1$),

$$U^{(j)}(y) = -\left(1 + b(1 + jy)\right) e^{jy},\ V^{(j)}(y) = \left(1 + bjy\right) e^{jy},\ Q^{(j)}(y) = 4\pi b e^{jy}$$

with $b = -\sqrt{2}$ for Problem I and $b = -(2 - \sqrt{2})$ for Problem II. With pre-stretch ($\lambda_0 > 1$),

$$U^{(j)}(y) = -b_1 e^{jy} - b_2 \lambda_0^{\,3} e^{j\lambda_0^3 y},\ V^{(j)}(y) = b_1 e^{jy} + b_2 e^{j\lambda_0^3 y},\ Q^{(j)}(y) = -2\pi(\lambda_0^{\,2} - \lambda_0^{\,-4}) b_1 e^{jy} \tag{4.3}$$

with $b_1 = (\lambda_0^{\,2} + \lambda_0^{\,-4} + \tau\,\Omega_C / 2) / (\lambda_0^{\,2} - \lambda_0^{\,-4})$ and $b_2 = -(2\lambda_0^{\,-4} + \tau\,\Omega_C / 2) / (\lambda_0^{\,2} - \lambda_0^{\,-4})$. In the limit $\lambda_0 \to 1$, the two linearly independent contributions in (4.3) become linearly dependent and, in that limit the first expressions apply.

4.1 Digression: The bifurcation functional for a finite thickness layer of Gent material

For completeness and because results for linear stability do not appear to be available in the literature, we include in this sub-section the quadratic bifurcation functional governing the linear stability of the finite thickness layers in Problems I and II. Moreover, we present the functional for Gent's (1996) generalization of the neo-Hookean material which introduces one extra 'stiffening' parameter J_L defined later in the paper in Section 6. With the same dimensionless variables introduced above such that the bottom of the layer is at $y \equiv -y_B = -2\pi h / \ell$ and modal displacements of the form, $(u_1, u_2) = (U(y) \sin x, V(y) \cos x)$ the functional is

$$\frac{\Delta\Psi_2}{\mu\ell^2}=\frac{\pi}{2}\int_{-y_B}^{0}\left\{M_1\left(U-V'\right)^2+M_2\left(U'-V\right)^2-\frac{\lambda_0^{\,2}(1-\lambda_0^{-6})}{\omega_0}\left(\frac{1}{2}\left(U'-V\right)^2+U^2-V^2\right)\right\}dy$$
$$+\frac{2\pi\gamma}{\mu\ell}V(0)^2-\frac{\pi}{2}\Omega\left(\tau U(0)V(0)+\operatorname{cotanh}(y_B)V(0)^2\right) \tag{4.4}$$

with $\omega_0=1-(2\lambda_0^{\,2}+\lambda_0^{-4}-3)/J_L$ and

$$M_1=\frac{\lambda_0^{\,2}}{2\omega_0}\left(1+\lambda_0^{-6}+(\lambda_0^{\,2}/\omega_0 J_L)(1-\lambda_0^{-6})^2\right),\ M_1=\frac{\lambda_0^{\,2}}{2\omega_0}\left(1+\lambda_0^{-6}\right)$$

The limit as $J_L\to\infty$ applies to the neo-Hookean material. Depending on how the functional is used, the incompressibility condition $V'+U=0$ may have to be enforced. The finite thickness of the layer enters (4.4) through the lower limit of integration, $y_B=2\pi h/\ell$, and through $\operatorname{cotanh}(y_B)$ in the electro-static energy contribution. In the short wavelength limit, $y_B\to\infty$ and $\operatorname{cotanh}(y_B)=1$. In deriving (4.4) for the Gent material we found it most convenient and efficient to use Hill's (1961) approach to bifurcation. By direct manipulation it is straightforward to show that the short wavelength limit of (4.4) for the neo-Hookean material is the same as what one obtains for $\Delta\Psi_2$ from (4.1).

4.2 The Koiter post-bifurcation analysis

The power of Koiter's (1945) initial post-bifurcation expansion method for the present problems is two-fold: (i) It enables a straightforward evaluation of the initial post-bifurcation behavior of the perfect system. (ii) By including the lowest order contribution of small imperfections to the energy functional, it permits and an assessment of the imperfection-sensitivity of the maximum attainable voltage. The Koiter method unites the behaviors of the perfect and imperfect systems. By making use of the results of the general analysis given in the Support Materials, it is possible to arrive at the desired results directly. However, to carry out this process it is first necessary to introduce some general notation to represent the energy functional in (4.1) for the perfect system.

Note that $\Delta\Psi$ is linear in the voltage parameter Ω and has a combination of quadratic and cubic terms in u, where the compact notation u for $(u_1, u_2, \Delta q)$ will be used. In this notation, the initial post-bifurcation expansion has the form

$$u = \sum_{j=1}^{N} \xi_j u^{(j)} + \Delta u \tag{4.5}$$

where the terms Δu are order ξ^2. Write (4.1) compactly as

$$\Delta\Psi(u, \Omega) = F_2(u) - \Omega\, G_2(u) + F_3(u) - \Omega\, G_3(u) \tag{4.6}$$

where F_i and G_i are homogeneous of degree i in u. Homogeneity allows one to introduce the following additional notation for F_2 with a similar notation for G_2:

$$\begin{aligned} &F_2(u_A + u_B) = F_2(u_A) + 2F_{11}(u_A, u_B) + F_2(u_B), \\ &F_{11}(u_A, u_B) = F_{11}(u_B, u_A) \;\; \& \;\; F_{11}(u_A, u_A) = F_2(u_A) \end{aligned} \tag{4.7}$$

In the general notation, the bifurcation modes have the same eigenvalue Ω_C and satisfy

$$\left.\begin{aligned} &\Delta\Psi_2(u^{(i)}, \Omega_C) = F_2(u^{(i)}) - \Omega_C G_2(u^{(i)}) = 0 \\ &\delta\Delta\Psi_2 = F_{11}(u^{(i)}, \delta u) - \Omega_C G_{11}(u^{(i)}, \delta u) = 0 \end{aligned}\right\} \tag{4.8}$$

for $i = 1, N$ and for all admissible variations δu. An orthogonality condition is needed to uniquely define the modes and the higher order terms Δu, and we require

$$F_{11}(u^{(i)}, u^{(j)}) = 0,\ i \neq j \;\; \& \;\; F_{11}(u^{(i)}, \Delta u) = 0,\ \ i = 1, N \tag{4.9}$$

It follows from (4.8) that

$$G_{11}(u^{(i)}, u^{(j)}) = 0,\ i \neq j \;\; \& \; G_{11}(u^{(i)}, \Delta u) = 0,\ \ i = 1, N \tag{4.10}$$

The general Koiter analysis presented in the Supporting Materials provides the following expansion of the energy functional which is accurate up to and including terms of order ξ^3:

$$\Delta\Psi = (\Omega_C - \Omega)\sum_{i=1}^{N}\xi_i^2 G_2(u^{(i)}) + F_3\left(\sum_{i=1}^{N}\xi_i u^{(i)}\right) - \Omega_C G_3\left(\sum_{i=1}^{N}\xi_i u^{(i)}\right) + O(\xi\bar{\xi}) \tag{4.11}$$

The contributions of the higher order terms Δu to this functional are of order ξ^4, and the terms denoted by $O(\xi\bar{\xi})$ are the lowest order contributions from the imperfections given below.

For the present problems the general analysis provides results for the initial post-bifurcation behavior directly in terms of the bifurcation modes without the need to evaluate higher order terms in the expansion. Translating from the abstract notation and evaluating the integrals involved in (4.11), one obtains

$$\begin{aligned}\frac{\Delta\Psi}{C\mu\ell^2} = (1-\Omega/\Omega_C)\sum_{j=1}^{6} j\xi_j^{\,2} + a_1\xi_1^{\,2}\xi_2 + a_2\xi_1\xi_2\xi_3 + a_3\xi_1\xi_3\xi_4 + a_4\xi_1\xi_4\xi_5 \\ + a_5\xi_1\xi_5\xi_6 + a_6\xi_2^{\,2}\xi_4 + a_7\xi_2\xi_3\xi_5 + a_8\xi_2\xi_4\xi_6 + a_9\xi_3^{\,2}\xi_6 + O(\xi\bar{\xi})\end{aligned} \tag{4.12}$$

where

$$C = \sqrt{2}\pi\Omega_C,\ \lambda_0 = 1$$

$$C = \pi\Omega_C\left(1-\tau(b_1+\lambda_0^{\,3}b_2)\right) = \pi\Omega_C\left(1-\tau\left(1-\lambda_0^{\,-3}-\tfrac{1}{2}\tau\lambda_0\Omega_C\right)(1-\lambda_0^{\,-3})^{-1}\right),\quad \lambda_0 > 1$$

All the nonzero terms for the first six modes ($N = 6$) have been listed in (4.12), and the values of the coefficients a_i are given in Table 1 for $\lambda_0 = 1,\ 2,\ 3$.

	a_1	a_2	a_3	a_4	a_5	a_6	a_7	a_8	a_9
$\lambda_0 = 1, \mathrm{I}$	17.1	64.5	103.0	150.6	206.7	52.8	154.6	212.1	107.0
$\lambda_0 = 1, \mathrm{II}$	-11.2	-47.6	-81.8	-125.0	-177.2	-41.0	-125.5	-178.2	-89.3
$\lambda_0 = 2, \mathrm{I}$	17.3	56.2	82.7	113.7	149.3	38.1	101.3	131.2	62.5
$\lambda_0 = 2, \mathrm{II}$	-18.7	-58.2	-82.7	-110.7	-142.5	-38.4	-98.8	-124.4	-59.1
$\lambda_0 = 3, \mathrm{I}$	28.2	84.6	115.8	149.6	186.0	52.5	128.9	155.8	72.8
$\lambda_0 = 3, \mathrm{II}$	-32.3	-95.4	-128.1	-162.8	-199.7	-60.1	-146.6	-175.1	-83.4

Table 1. Post-bifurcation coefficients for Problems I and II for the first six modes ($N=6$) for no pre-stretch, $\lambda_0=1$, and pre-stretches $\lambda_0=2$ & 3.

Accounting for the effect of small imperfections is an important aspect of Koiter's theory of elastic stability, and his thesis (Koiter, 1945) and the book on Koiter theory (van der Heijden, 2009) deal with the introduction of imperfections at some length. In an investigation of the stability of Biot surface wrinkling, Cao and Hutchinson (2012) present a systematic derivation of the modification of the energy functional that accounts for initial surface undulations. Two types of imperfections will be considered here: stress-free initial sinusoidal undulations of the layer top surface for cases in which there is no pre-stretch, and small sinusoidal vertical perturbing forces for all cases including pre-stretch. The combined loadings, pre-stretch and the electrostatic, makes the analysis of the effect of initial geometric surface undulations difficult. Moreover, tensile pre-stretch tends to smooth out initial surface undulations rendering them less potent. Other types of imperfections are likely to be more important when there is appreciable pre-stretch. For the second type of imperfection we have considered one that is much easier to analyze—a perturbing surface force. For both types of imperfection, only the lowest order contributions, $O(\xi\overline{\xi})$, of small imperfections to the energy functional will be considered. Derivation details are in the Supporting Materials.

For the layers with no pre-stretch we consider geometric imperfections in the form of initial stress-free surface undulations, $\overline{u}_2(x_1,0)$:

$$\begin{aligned}&\overline{u}_2(x_1,0)=\ell\sum_{i=1}^{N}\overline{\xi}_i^{\,G}\cos(2\pi i x_1/\ell) \qquad \text{(dimensional)}\\ &\overline{v}(x)=\overline{u}_2(x_1,0)/\ell=\sum_{i=1}^{N}\overline{\xi}_i^{\,G}\cos(ix) \qquad \text{(dimensionless)}\end{aligned} \tag{4.13}$$

with $\overline{\xi}_j^{\,G}$ as the j^{th} imperfection amplitude. The lowest order contribution of the geometric imperfection to the energy functional $\Delta\Psi$ in (4.11) is

$$-2\Omega\sum_{i=1}^{N} i\xi_i\overline{\xi}_i^{\,G}G_2(u^{(i)})=-2\mu\ell^2C(\Omega/\Omega_C)\sum_{i=1}^{N} i\xi_i\overline{\xi}_i^{\,G} \tag{4.14}$$

The second type of imperfection considered (with and without pre-stretch) is an independently prescribed small periodic vertical force/area distribution applied to the surface to perturb the system

$$\begin{aligned} p &= 4C\mu\sum_{i=1}^{N}\overline{\xi}_i^P\cos(2\pi i x_1/\ell) \qquad \text{(dimensional)} \\ p/\mu &= 4C\sum_{i=1}^{N}\overline{\xi}_i^P\cos(ix) \qquad\quad \text{(dimensionless)} \end{aligned} \tag{4.15}$$

Here, p is positive upward and prescribed per unit area in the pre-bifurcation state, with $\overline{\xi}_i^P$ as the dimensionless amplitude of i^{th} imperfection component. The coefficient $4C$ has been introduced as a factor to align this imperfection to the geometric imperfection. The potential energy contribution to the energy functional $\Delta\Psi$ in (4.11) due to the prescribed perturbing force p is

$$-\int_{-\ell/2}^{\ell/2} p u_2(x_1,0)dx_1 = -2\mu\ell^2 C\sum_{j=1}^{N}\xi_j\overline{\xi}_i^P \tag{4.16}$$

The geometric imperfection and perturbing force imperfection contributions to $\Delta\Psi/(C\mu\ell^2)$ in (4.12) are respectively: $-2(\Omega/\Omega_C)\sum_{i=1}^{N} i\xi_i\overline{\xi}_i^G$ and $-2\sum_{i=1}^{N}\xi_i\overline{\xi}_i^P$. Thus, when there is no pre-stretch and when the only the first imperfection components, $\overline{\xi}_1^G$ and $\overline{\xi}_1^P$, are nonzero, the two imperfections will produce identical results for the maximum sustainable voltage gradient in the asymptotic limit of small imperfections (when $\Omega/\Omega_C \cong 1$) if $\overline{\xi}_1^P = \overline{\xi}_1^G$.

5. Initial post-bifurcation behavior, including small imperfections

The post-bifurcation equilibrium equations follow directly by rendering (4.12) stationary with respect to the mode amplitudes, i.e., $\partial\Delta\Psi/\partial\xi_j = 0$ for $j = 1, N$. The 2-mode approximation reveals the essence of the behavior for the perfect system and the effect of small imperfections. For $N = 2$, the equilibrium equations with the geometric imperfection are

$$\begin{aligned}(1-\Omega/\Omega_C)\,\xi_1 + a_1\xi_1\xi_2 &= (\Omega/\Omega_C)\overline{\xi}_1^G \\ (1-\Omega/\Omega_C)\,\xi_2 + \tfrac{1}{4}a_1\xi_1^2 &= (\Omega/\Omega_C)\overline{\xi}_2^G\end{aligned} \tag{5.1}$$

with $a_1 = 17.1$ for Problem I and $a_1 = -11.2$ for Problem II for no pre-stretch. The cubic term in the energy functional (4.11) which gives rise to the nonlinear coupling between the modes is $\xi_1^2\xi_2$. This term is present because the integral of the product of x-dependent terms such as $\cos(x)^2\cos(2x)$ is non-zero, while the x-dependences of the terms ξ_1^3, ξ_2^3 and $\xi_1\xi_2^2$ integrate to zero.

The bifurcation solutions to (5.1) for the perfect system ($\overline{\xi}_1 = \overline{\xi}_2 = 0$) are

$$\xi_1 = \pm 2(1-\Omega/\Omega_C)/a_1, \quad \xi_2 = -(1-\Omega/\Omega_C)/a_1 \tag{5.2}$$

The solutions are plotted in Fig. 7 for the two problems. All the solutions above Ω_C are unstable, including the perfectly flat state, and these solutions cannot be realized physically. The initial post-bifurcation solutions associated with $\Omega < \Omega_C$ are also instable. If the voltage gradient of the perfect system attains Ω_C and remains fixed at that level, no other nearby equilibrium states exist and almost any perturbation would cause the system will snap dynamically to a remote state. The present analysis is only valid for small deflection amplitudes (and sufficiently small imperfection amplitudes) and cannot be used to predict the finite strain state to which the system snaps. Further discussion of the stable post-bifurcation states such as creases-like or ridge-like entities will be given in the next section. The unstable equilibrium solutions for the perfect system in Fig. 7 for $\Omega < \Omega_C$ are physically relevant however because they determine the behavior of the system in the presence of small imperfections, as Koiter established. This point is illustrated in Fig. 7 where solutions to (5.1) are plotted for small imperfections ($\overline{\xi}_1^G \neq 0$, $\overline{\xi}_2^G = 0$). For Problem I, the relevant sign of the imperfection is $\overline{\xi}_1^G < 0$, which drives the trough of the surface deflection towards the electrode at the bottom of the layer (see Fig. 8). By contrast, for Problem II, imperfections with $\overline{\xi}_1^G > 0$ drive the peak deflection towards the electrode which lies above the top surface of the elastomer. The solution for each imperfect

system is stable as the voltage is increased from zero until the local maximum voltage, $\Omega_{\max}$, is attained.

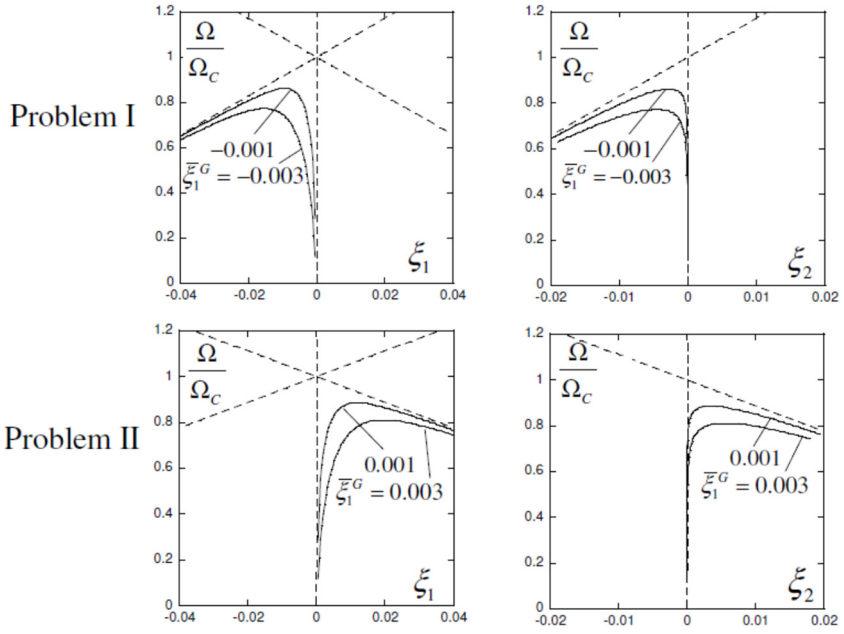

Fig. 7 Initial post-bifurcation behavior of the perfect system and the influence of small geometric imperfections (4.13) for the 2-mode approximation for Problems I and II ($\lambda_0 = 1$). The solutions for the perfect system (5.1) shown as dashed lines emanating from the bifurcation point at $\Omega = \Omega_C$.

The expression (in dimensional quantities) for the vertical displacement along the top surface of the elastomer for the two-mode approximation using (5.2) for the perfect system is

$$u_2(x_1,0) = \ell(\xi_1 u_2^{(1)} + \xi_2 u_2^{(2)}) = -(1-\Omega/\Omega_C)\ell\left(2\cos(2\pi x_1/\ell) + \cos(4\pi x_1/\ell)\right)/a_1 \qquad (5.3)$$

This is plotted for the two problems in Fig. 8 as $(u_2(x_1,0)/\ell)/[(1-\Omega/\Omega_C)]$ vs. x_1/ℓ for one period. (The other choice of sign for the contribution from ξ_1 simply translates this combination of modes by a half-wavelength and need not be shown.) On the bifurcation solution with $\Omega/\Omega_C < 1$, the surface deflection penetrates downward towards the electrode on the bottom of the layer for Problem I, but it reaches upward towards the fixed planar electrode for Problem II. The vertical surface deflection $u_2(x_1,0)$ has been computed for each N-mode approximation up

to $N=6$. In each of these approximations $u_2(x_1,0)$ is proportional to $(1-\Omega/\Omega_C)$, and plots of these results are also included in Fig. 8. The present analysis, which accounts for the lowest order nonlinear interaction among modes following bifurcation, predicts the emergence of a peak deflection of the elastomer surface directed towards the other electrode. For Problem I, it reveals that localization of the modes into a relatively sharp open valley, while for Problem II, a ridge emerges. The important conclusion is that multiple mode interaction generates open crease-like or rounded ridge-like modes not the sinusoidal wrinkling mode generally expected from a conventional linear stability analysis.

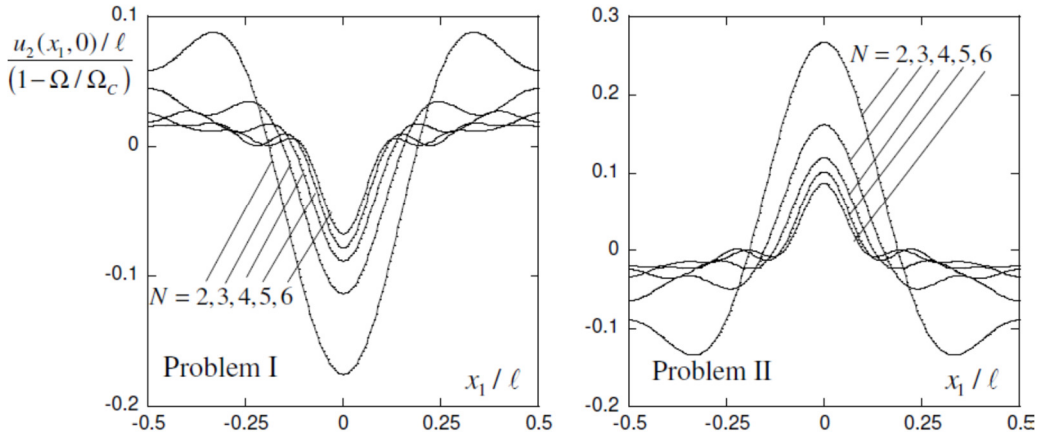

Fig. 8 Initial post-bifurcation mode shapes for one period for modal approximations from $N=2$ to $N=6$ for Problems I and II. The normalized vertical deflection at the top surface of the elastomer is shown.

The maximum voltage the system can sustain in the presence of small geometric imperfections can be analyzed for the 2-mode approximation (5.1). For $\bar{\xi}_1^G \neq 0$ and $\bar{\xi}_2^G = 0$, one finds

$$\left(1-\frac{\Omega_{\max}}{\Omega_C}\right)^2 = \frac{3\sqrt{3}}{4}\frac{\Omega_{\max}}{\Omega_C}(-a_1\bar{\xi}_1^G), \quad (\bar{\xi}_1^G<0,\ \text{Problem I};\ \bar{\xi}_1^G>0,\ \text{Problem II}) \tag{5.4}$$

while for $\bar{\xi}_1^G = 0$ and $\bar{\xi}_2^G \neq 0$, one finds

$$\left(1-\frac{\Omega_{\max}}{\Omega_C}\right)^2 = \frac{\Omega_{\max}}{\Omega_C}(-a_1\bar{\xi}_2^G), \quad (\bar{\xi}_2^G<0,\ \text{Problem I};\ \bar{\xi}_2^G>0,\ \text{Problem II}) \tag{5.5}$$

Through their dependency on a_1, these formulas drive home the relevance of the initial post-bifurcation behavior of the perfect system. The result (5.4) for $\overline{\xi}_1^G \neq 0$ and $\overline{\xi}_2^G = 0$ is plotted in Fig. 9. This figure includes the predictions for the maximum attainable voltage for all the modal approximation derived from (4.12) for $N = 2, 6$. What the 2-mode solution lacks in accuracy, it makes up for in its simplicity, capturing many of the essential features of the behavior as has been previously asserted. It must be emphasized again that these are asymptotic results valid only for sufficiently small imperfections. Nevertheless, they imply an extreme sensitivity to very initial small surface undulations with amplitudes on the order of only $10^{-3}\ell$ to $10^{-2}\ell$. Analytically, the source of this exceptionally strong dependence can be seen from (5.4), which for $\left|\overline{\xi}_1\right| << 1$ can be expressed as

$$\frac{\Omega_{\max}}{\Omega_C} = 1 - \sqrt{\frac{3\sqrt{3}}{4}(-a_1\overline{\xi}_1^G)} \quad , \quad -a_1\overline{\xi}_1^G \geq 0 \tag{5.6}$$

Next, consider the force-perturbing imperfection, $p/\mu = 4C\overline{\xi}_1^P \cos x$ with $\overline{\xi}_j = 0,\ j \geq 2$ for which the contribution to the energy functional (4.12) is $-2\xi_1\overline{\xi}_1^P$. If there is no pre-stretch, this can be compared with the corresponding contribution from the geometric imperfection $-2(\Omega/\Omega_C)\xi_1\overline{\xi}_1^G$. As noted, for small imperfections, the force-perturbing imperfection is asymptotically equivalent to the geometry imperfection if $\overline{\xi}_1^P = \overline{\xi}_1^G$. Indeed, the two-mode approximation derived from (4.12) for this case predicts precisely

$$\frac{\Omega_{\max}}{\Omega_C} = 1 - \sqrt{\frac{3\sqrt{3}}{4}(-a_1\overline{\xi}_1^P)} \quad , \quad -a_1\overline{\xi}_1^P \geq 0 \tag{5.7}$$

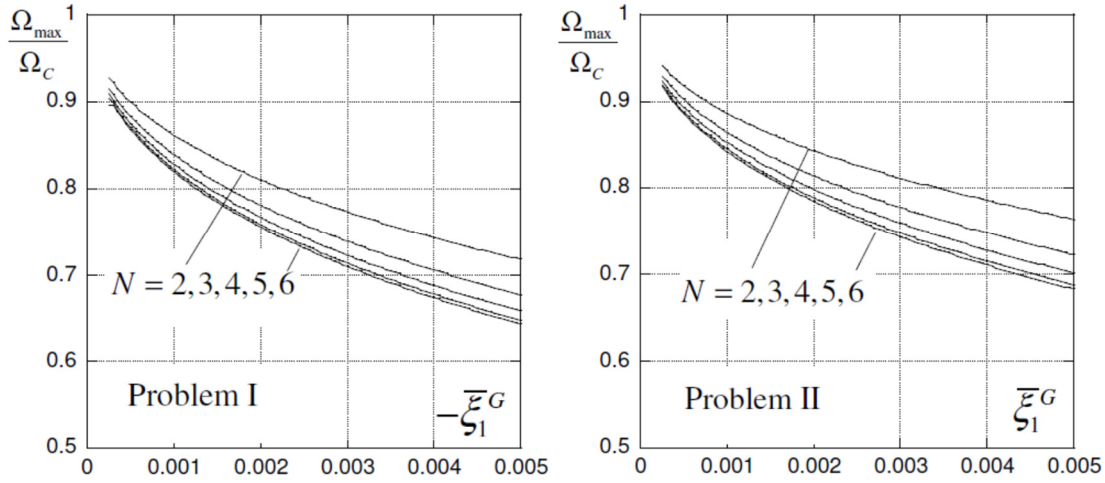

Fig. 9 Imperfection-sensitivity for Problems I and II with no pre-stretch ($\lambda_0 = 1$) showing the maximum attainable value of the voltage parameter computed using the modal approximations for $N = 2,6$. The geometric imperfection is an initial undulation of the top surface of the elastomeric layer with vertical displacement $\bar{u}_2(x_1,0) = \overline{\xi}_1 \ell \cos(2\pi x_1/\ell)$. ($\overline{\xi}_j = 0,\ j \geq 2$).

The effect of pre-stretch on imperfection-sensitivity is displayed in Fig. 10 for the perturbing force imperfection where for each of the two problems, differences in λ_0 produce a relatively modest change in the ratio Ω_{max}/Ω_C. The pre-stretch has a larger influence on the critical bifurcation voltage of the perfect system, Ω_C, as seen in Fig. 5. The main conclusion, however, is these results imply that the strong imperfection-sensitivity is not significantly affected by pre-stretch at least not for the perturbing force imperfection. Fig. 11 plots the maximum attainable dimensionless voltage gradient for Problem I as a function of pre-stretch for the perfect layer and for two levels of the perturbing force imperfection.

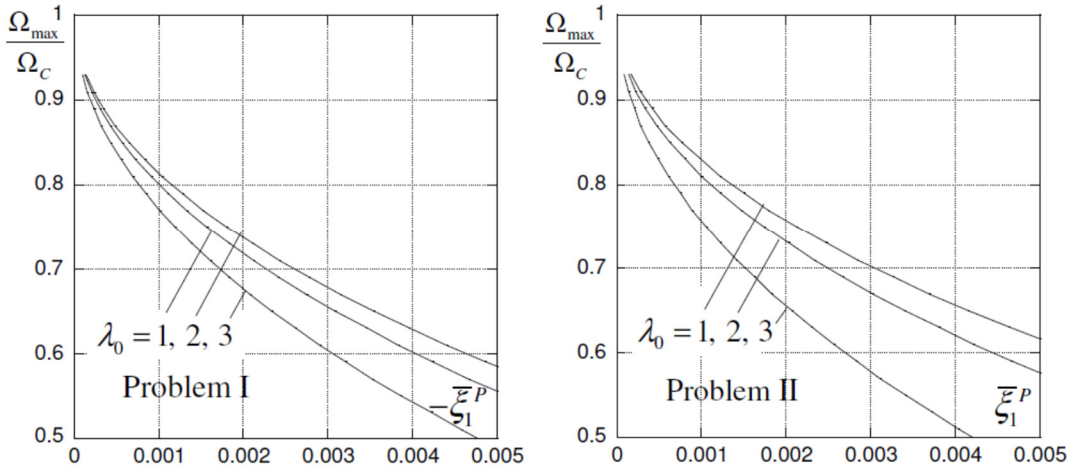

Fig. 10 Effect of pre-stretch λ_0 on the imperfection-sensitivity of the maximum attainable value of the voltage parameter computed using the 6-mode approximation ($N=6$). The imperfection is a prescribed vertical force perturbation applied to the top surface of the elastomeric layer with vertical force/area $p=4C\mu\bar{\xi}_1^P\cos(2\pi x_1/\ell)$, ($\bar{\xi}_j^P=0,\ j\geq 2$). The dependence of Ω_C on λ_0 is seen in Fig. 5.

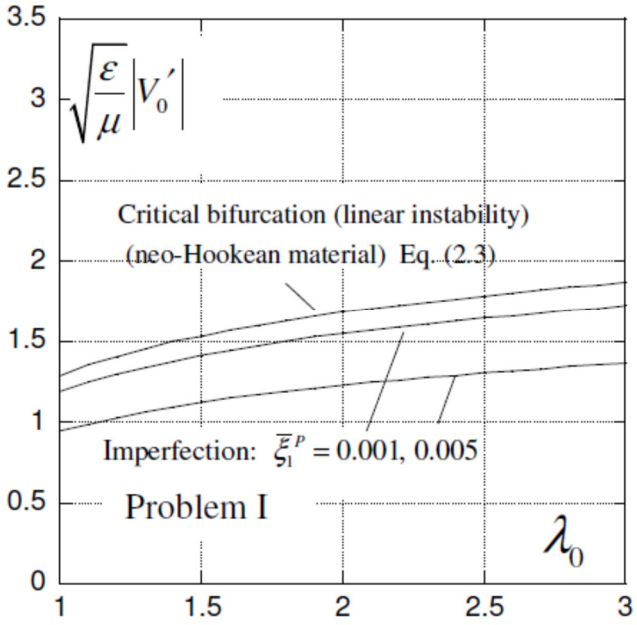

Fig. 11 The effect of the perturbing force imperfection on the maximum attainable voltage as a function of biaxial pre-stretch for Problem I.

6. Comparison with experiments and the threshold for creasing for Problem I

Before discussing related experiments and numerical results for creasing, we first present additional bifurcation results which will provide insights into the applicability of the neo-Hookean material for modeling the constrained elastomeric layers in Problems I and II when pre-stretch is present. For this purpose, we make use of the Gent (1996) generalization of the neo-Hookean model (3.1) with energy density function

$$W = -\frac{1}{2}\mu J_L \ln\left(1-(\lambda_I^{\,2}+\lambda_{II}^{\,2}+\lambda_{III}^{\,2}-3)/J_L\right) \tag{6.1}$$

which is also subject to the constraint $\lambda_I\lambda_{II}\lambda_{III}=1$. The single additional parameter in the Gent model, J_L, introduces incremental stiffening with increasing deformation and limits the stretches to the range $(\lambda_I^{\,2}+\lambda_{II}^{\,2}+\lambda_{III}^{\,2}-3)<J_L$. With $J_L\to\infty$ the neo-Hookean model is recovered. Fig. 12 shows the influence of the Gent parameter, J_L, on the critical voltage plotted as a function of the equi-biaxial pre-stretch, λ_0, for the short wavelength bifurcation modes for the two problems of interest here. With no pre-stretch ($\lambda_0=1$), the Gent parameter has no influence on the critical bifurcation voltage because the pre-bifurcation state is purely hydrostatic. However, depending on its value, the Gent parameter has an appreciable effect on the critical voltage at pre-stretches as low as $\lambda_0=1.5$ or 2, and this is pertinent to the discussion which follows.

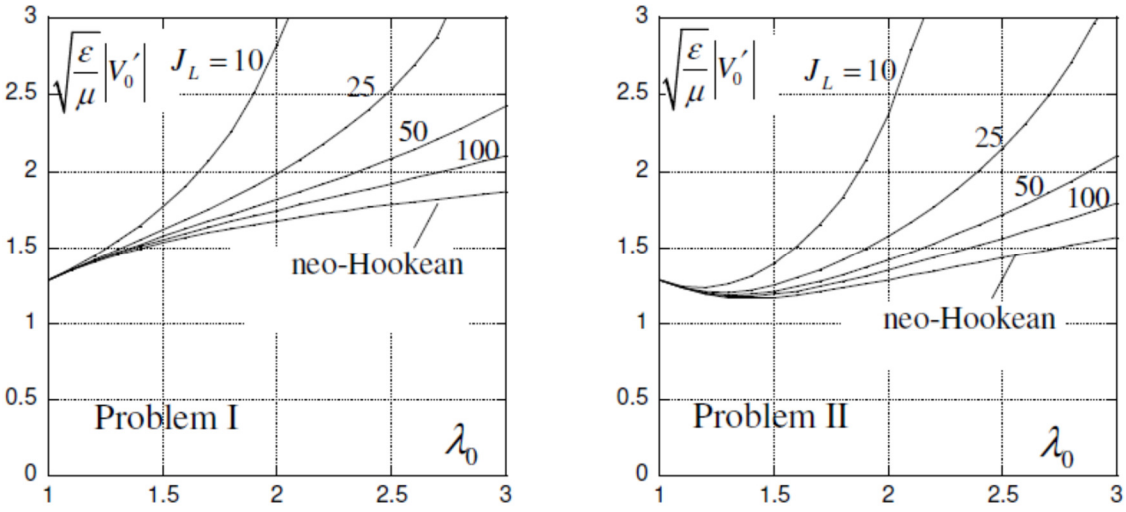

Fig. 12 The critical voltage for short wavelength bifurcations for Problems I and II as a function of the equi-biaxial pre-stretch, λ_0, with $\gamma = 0$ as predicted by the Gent model for four values of J_L and the limit for the neo-Hookean model. The calculation procedure for these results is described in the Supporting Materials.

Fig. 13 is drawn from Fig. 3 of the paper on Problem I by Wang et al. (2011a) which contains both experiments and finite element simulations of the threshold condition for creasing. The experimental data points in Fig. 13 represent the voltage gradient (critical electric field) at which crease-like features are first observed on the surface of the layer—sinusoidal surface wrinkles were not observed. The threshold condition for creases as a function of pre-stretch was computed by Wang et al. (2011a) for a neo-Hookean material as the lowest voltage gradient for which the system energy is the same for a creased state and the uniform state. For reference in the discussion that follows, note that Fig. 11 presents the critical voltage at wrinkling bifurcation (linear instability) and the voltage maximum for two levels of imperfection as a function of pre-stretch for Problem I from the present analysis for the neo-Hookean material.

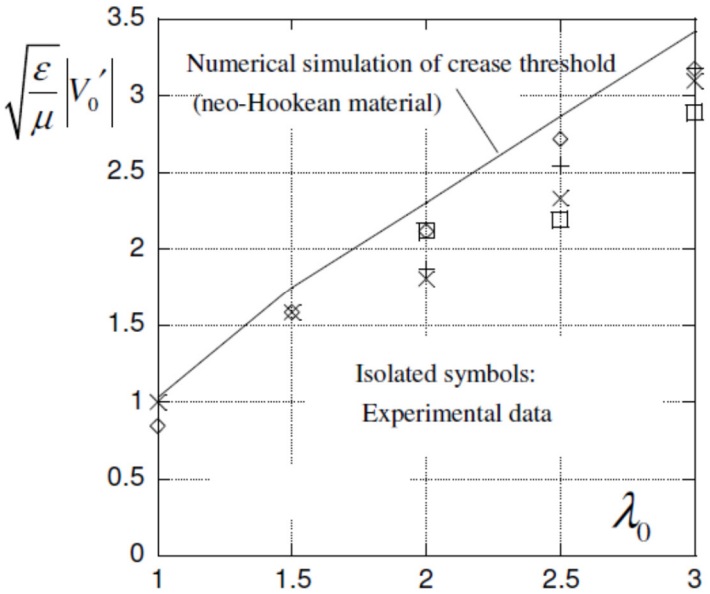

Fig. 13 Experimental data on the critical voltage parameter and numerical simulation of the creasing threshold as a function of equi-biaxial pre-stretch for Problem I extracted from Fig. 3 of Wang et al. (2011a). The finite element simulations of the creasing threshold assumed a neo-Hookean material. The experimental data points represent a range of layer thicknesses $(40-200\mu m)$ and shear moduli $(10-200kPa)$.

With no pre-stretch, the experimental values are in the range, $0.85 \le \sqrt{\Omega} \le 1.0$ and the computed crease threshold is $\sqrt{\Omega} = 1.03$. The critical bifurcation voltage gradient for wrinkling of the perfect system from the present paper is $\sqrt{\Omega} = 1.287$, and in the presence of an imperfection amplitude, $\overline{\xi}_1^G \cong \overline{\xi}_1^P = -0.005$, the present analysis predicts crease-like mode shapes and a maximum voltage given by $\sqrt{\Omega} \cong 0.9$. Thus, with no pre-stretch, the experiments and crease threshold analysis of Wang et al. (2011a) align reasonably well with the predictions of the present analysis. These values also line up in a manner consistent with expectations based on prior extensive experience with the plane strain compression of a neo-Hookean layer: namely, experimental observations and threshold condition for creasing fall roughly 25% below Biot's bifurcation result for surface wrinkling (Wei et al., 2009). To our knowledge, measurements of initial surface undulations have not been made which would allow a direct assignment of values for amplitudes of the geometric imperfections. Nevertheless, the choice $\overline{\xi}_1^G = -0.005$ is indirectly corroborated by the fact that the analysis of Cao and Hutchinson (2012) of the instability of Biot surface wrinkling shows that imperfection amplitudes in this same range predict crease-like modes at compression levels in agreement with observations.

While the present results appear to be fully consistent with the theoretical and experimental results on creasing, there are some clear inconsistencies among the two sets of results for non-zero pre-stretches as will now be discussed. First note the inconsistency between the critical voltage for onset of surface wrinkles predicted by the bifurcation analysis for the neo-Hookean material in Fig. 11 and the critical voltage threshold for creasing predicted by the numerical computation for the same material in Fig. 13. The latter exceeds the former for all the nonzero pre-stretches shown, i.e., $\lambda_0 \ge 1.5$, while there is every reason to expect from prior experience with surface instabilities on compressed elastomers that the opposite should be true. The fact that wrinkling bifurcation is predicted to be highly unstable also strongly suggests that the creasing threshold should fall below wrinkling bifurcation. The unexpected juxtaposition of the wrinkling bifurcation and the creasing threshold is unresolved. Of course, the present bifurcation result could be in error. With this in mind, we have made every effort to ensure that

(2.3) is indeed exact (see Supporting Materials), but independent verification would be welcomed.

Another fundamental inconsistency is that the experimental results for the critical voltage gradient for creasing of the pre-stretched layer in Fig. 13 are greater than critical voltage gradient at bifurcation for surface wrinkling in Fig. 11, in some cases significantly so. This is physically implausible and mathematically unexpected because, as just noted, the bifurcation is predicted to be extremely unstable. It seems likely this discrepancy can be explained by limitations of the neo-Hookean model when non-negligible pre-stretch is involved. As seen in Fig. 12a, the Gent parameter, J_L, has a significant influence on the bifurcation predictions in the presence of pre-stretch. The stiffening captured by Gent model has been shown to have a strong influence on surface wrinkling and creasing for compressed elastomeric layers by Jin and Suo (2015). For equi-biaxial pre-stretch, λ_0, the invariant in (6.1) is $\lambda_I^2 + \lambda_{II}^2 + \lambda_{III}^2 = 2\lambda_0^2 + \lambda_0^{-4}$ which becomes large enough to produce elevations of the voltage at bifurcation in Fig. 12a for all but very large values of the Gent parameter. A Gent parameter on the order of $J_L = 20$ would produce critical bifurcation voltages consistently above the experimental data points in Fig. 13.

7. Concluding remarks

The nonlinear interaction among the simultaneous linear stability modes associated with critical voltage gives rise to the highly unstable bifurcation behavior and strong sensitivity of the maximum attainable voltage to imperfections in the system. Mode interaction results in modal shapes that are more crease-like, or ridge-like, than the sinusoidal wrinkle shape associated with a single linear mode. Structural systems which display multi-mode buckling behavior are the cylindrical shell under axial compression (Koiter, 1945) and the spherical shell under external pressure (Hutchinson, 1967). In the world of structures, these two shell/loading combinations are notorious for their imperfection-sensitivity and are traditionally designed to carry no more than about 20% of the load predicted for the perfect structure, i.e., 20% of the load at loss of linear stability. The shell problems differ from the problems analyzed here and from the surface instability of compressed elastomers in one important respect. While the wavelengths of the instability modes in the latter problems can be arbitrarily short (limited by additional intervening physics such as surface energy), the buckle wavelengths in the shell problems are limited by the

bending stiffness of the shell and are long compared to the shell thickness. Short wavelength instability modes analogous creases or ridges do not arise in shell buckling problems if the material is elastic.

The comparisons laid out in Section 6 clearly point to the need for better characterization of the crease threshold for Problem I or, possibly, a correction in the critical bifurcation when pre-stretch is present. To our knowledge, the threshold condition for the analogous ridge (or anti-crease) in Problem II, has not been analyzed for elastomeric materials. As previous experience with creasing of compressed elastomer surfaces has amply revealed, these are challenging computational problems requiring accurate finite strain resolution and, depending on how the simulations are conducted, the introduction of small initial imperfections and sophisticated computational techniques to follow unstable equilibrium paths. Based on the current existing experimental data base in Fig. 13, we have also argued that it seems likely that the neo-Hookean material model cannot adequately characterize the material response in this application if significant pre-stretch is present.

Further motivation for gaining a better quantitative understanding of the post-bifurcation states and how they evolve with changes in electric field derives from recent work suggesting a richness not only of the instability patterns (Wu and Russel, 2009; van den Ende et al., 2013) but in the variety of the states themselves. Experiments (Wang et al., 2011b, 2013) have revealed that creases evolve into cylindrical crater or pit-like entities. Shian and Clarke (2016, 2018) have exploited these phenomena to design and test elastomer 'windows' with the arrangement of Problem I that can be tuned to be clear or cloudy by varying the applied electric field. An increasing electric field nucleates a few creases followed by an increasing areal density of creases with a further evolution into cylindrically shaped pits, all of which conspire to produce increasing cloudiness (Shian and Clarke, 2018). Transparency of the window returns when the electric field is removed. One clear challenge is the quantitative simulation of the sequence of post-bifurcation instability states and their relation to the electric field.

Acknowledgements. The author is indebted to his colleagues, David Clarke and Zhigang Suo, and to Qiming Wang and Xuanhe Zhao, who called attention to recent relevant papers on electrostatically driven instabilities and who provided insightful comments on the present paper.

References

Biot, M. A., 1963. Surface instability of rubber in compression. Appl. Sci. Res. 12, 168–182.

Biot, M. A., 1965. *Mechanics of incremental deformation*. New York, NY: Wiley.

Cao, Y-P., Hutchinson, J. W., 2012. From wrinkles to creases in elastomers: the instability and imperfection-sensitivity of wrinkling, Proc. R. Soc. A 468, 94-115.

Clarke, D.R., Hutchinson, J. W., 2021. On the electro-mechanical stability of elastomeric coaxial fibers, J. Appl. Mech. 88, 061005, 1-9.

Gent, A.N.,1996. A new constitutive relation for rubber. Rubber Chem.Technol. 69, 59–61.

Hill, R., 1961. Bifurcation and uniqueness in nonlinear mechanics of continua. Muskhelishvili Volume, Soc. Ind. Appl. Math., Philadelphia, Pennsylvania. 155-164.

Hohlfeld, E. B., 2008. Creasing, post-bifurcations and the spontaneous breakdown of scale invariance. PhD thesis, Harvard University, Cambridge, MA.

Hohlfeld, E. B., Mahadevan, L., 2011. Unfolding the sulcus. Phys. Rev. Lett. 106, 105702. (doi:10.1103/PhysRevLett.106.105702)

Huang, R., 2005. Electrically induced surface instability of a conductive thin film on a dielectric substrate, Appl. Rhys. Letters 87, 151911.

Hutchinson, J. W. 1967 Imperfection sensitivity of externally pressurized spherical shells. J. Appl. Mech. 34, 49–55.

Jin, L., Suo, Z., 2015. Smoothening creases on surfaces of strain-stiffening materials, J. Mech. Phys. Solids 74, 68-79.

Kofod, G., Kornbluh, R., Pelrine, R., Sommer-Larson, P., 2003. Actuation response of polyacrylate dielectric elastomers, J. Intel. Mater. Systems Struct. DOI: 10.1177/104538903039260

Koiter, W. T., 1945. *On the stability of elastic equilibrium* (in Dutch with English summary). Thesis Delft, H. J. Paris, Amsterdam. An English translation is available online see http://imechanica.org/node/1400.

Lu, T., Cheng, S., Li, T., Wang, T., Suo, S., 2016. Electromechanical catastrophe, Int. J. Appl. Mech. 8, 1640005 (14 pages).

Lu, T. Ma, C.., Wang, T., 2020. Mechanics of dielectric elastomer structures: A review, Extreme Mechanics Letters 38, 100752.

Park, H.S., Wang, Q., Zhao, X., Klein, P.A., 2013. Electromechanical instability on dielectric polymer surface: Modeling and experiment, Comput. Methods Appl. Mech. Engrg. 260, 40-49.

Plante, J.S., Dubowsky,S., 2006. Large-scale failure modes of dielectric elastomer actuators. Int. J. Solids and Struct. 43, 7727-7751.

Shian, S., Clarke, D. R., 2016. Electrically-tunable surface deformation of a soft elastomer, Soft Mater. DOI: 10.1039/c6sm00090h

Shian, S., Kjeer, P., Clarke, D. R., 2018. Electric-field induced surface instabilities of soft dielectrics and their effects on optical transmittance and scattering, J. Appl. Phys. 123, 113105.

Suo, Z., 2010. Theory of dielectric elastomers, Acta mech. Solids Sinica 28, 549-578.

Tanaka, T., Sun, S.-T., Hirokawa, Y., Katayama, S., Kucera, J., Hirose, Y., Amiya, T., 1987. Mechanical instability of gels at phase transformation. Nature **325**, 796–798.

van den Ende, D., Kamminga, J-D., Boersma, A., Andritsch, T., Steeneken, P. G., 2013. Voltage-controlled surface wrinkling of elastomeric coatings, Adv. Mater. 25, 3438-3442.

van der Heijden, A. M. A., 2009. *Elastic stability of solids and structures*. Cambridge, UK: Cambridge University Press.

Wang, Q., Tahir, Zhang, L., Zhao, X., 2011a. Electro-creasing instability in deformed polymer experiments and theory, Soft Mater. 14, https://doi.org/10.1039/C1SM05645J

Wang, Q, Zhang, L. Zhao, X., 2011b. Creasing to cratering instabilities in polymers under ultrahigh electric fields, Phys. Rev. Letters. 106, 118301.

Wang, Q., Zhao, X., 2013. Creasing-wrinkling transition in elastomer films under electric fields, Phys. Rev. E 88, 042403.

Wei, H., Zhao, X., Suo, Z., 2009. Formation of ceases on the surfaces of elastomers and gels, Appl. Phys. Letters 95, 111901.

Wu, N., Russel, W. B., 2009. Micro- and nano-patterns created via electrohydrodynamic instabilities, Nano Today 4, 180-192.

Supporting Materials

Surface instabilities of constrained elastomeric layers subject to electro-static stressing

John W. Hutchinson

School of Engineering and Applied Sciences,

Harvard University, Cambridge, MA, 02138

In these Supporting Materials the equation numbers will be prefaced by the initials SM, and equation numbers without this preface refer to the equations in the primary text. The references cited in this document are listed at the end of the primary text. We begin by filling in some details of the bifurcation analysis of the finite thickness layers, including discussion of the short wavelength limit, anticipating results from the second part of this document on development of the free energy functional and the post-bifurcation analysis for the short wavelength limit.

Bifurcation (linear stability) analysis including pre-stretch and surface energy

We begin with the quadratic bifurcation functional written for the finite thickness layer from Section (4.1). Here, the dimensionless coordinates are $(x, y) = (kx_1, kx_2)$, and the dimensionless displacements are taken to be the dimensional ones divided by $\ell = 2\pi / k$, i.e., $(u_1 / \ell, u_2 / \ell)$ becoming (u_1, u_2). Recall that the horizontal and vertical displacements of material points at (x_1, x_2) in the pre-stretched, pre-bifurcation, state, $\big(u_1(x_1, x_2), u_2(x_1, x_2)\big)$, are employed. The dimensionless quadratic bifurcation function for one periodic section per unit length in the x_3 direction is

$$\begin{aligned}\frac{\Delta\Psi_2}{\mu\ell^2} = \int_{-y_B}^{0}\int_{-\pi}^{\pi}\Big\{&\tfrac{1}{2}\lambda_0^{\,2}\left(u_{1,x}{}^2 + u_{2,x}{}^2\right) + \tfrac{1}{2}\lambda_0^{-4}\left(u_{1,y}{}^2 + u_{2,y}{}^2\right)\\ &-\left(\lambda_0^{-4} + \tfrac{1}{2}\tau\Omega\right)\left(u_{1,x}u_{2,y} - u_{1,y}u_{2,x}\right) - \Delta q(u_{1,x} + u_{2,y})/2\pi\Big\}\,dxdy\\ &+ 2\pi\frac{\gamma}{\mu\ell}\int_{-\pi}^{\pi} u_2(x,0)_{,x}{}^2\,dx - \frac{\pi}{2}\Omega\sum_{j=1}^{\infty}\operatorname{cotanh}(jy_B)\,j\,v_j^{\,2}\end{aligned} \tag{SM-1}$$

with $\tau = 1$ for Problem I and $\tau = -1$ for II, $y_B = 2\pi h / \ell$, and $v_j = 2\int_{-\pi}^{\pi} u_2(x,0)\cos(jx)dx$.

One can proceed in several ways. The procedure used here is as follows. In the first step, generate the linear system of pde's and boundary conditions that render $\Delta\Psi_2$ stationary

subject to $u_1(x,-y_B)=u_2(x,-y_B)=0$. The details of this step are omitted here but we use the fact that these pde's, boundary conditions and the periodicity requirement admit separated solutions of the form

$$u_1=U(y)\sin x,\ u_2=V(y)\cos x,\ \Delta q=Q(y)\cos x \tag{SM-2}$$

Substitution of these back into (SM-1) and evaluation of the integrations with respect to x gives

$$\begin{aligned}\frac{\Delta\Psi_2}{\mu\ell^2}=\pi\int_{-y_B}^{0}\left\{\tfrac{1}{2}\lambda_0^{\,2}\left(U^2+V^2\right)+\tfrac{1}{2}\lambda_0^{-4}\left(U'^2+V'^2\right)-\left(\lambda_0^{-4}+\tfrac{1}{2}\tau\Omega\right)\left(UV'+U'V\right)-Q(U+V')/2\pi\right\}dy\\ +2\pi^2\frac{\gamma}{\mu\ell}V(0)^2-\frac{\pi}{2}\Omega\,\mathrm{cotanh}(y_B)V(0)^2\end{aligned} \tag{SM-3}$$

with $(\,)'=d(\,)/dy$. Rendering $\Delta\Psi_2$ stationary with respect to U, V and Q subject to $U(-y_B)=0$ and $V(-y_B)=0$ requires

$$\left.\begin{aligned}&\lambda_0^{-4}U''-\lambda_0^{\,2}U+Q/2\pi=0\\&\lambda_0^{-4}V''-\lambda_0^{\,2}V-Q'/2\pi=0\\&U+V'=0\end{aligned}\right\}\ \text{for}\ \ -y_B\le y\le 0 \tag{SM-4}$$

$$\left.\begin{aligned}&\lambda_0^{-4}U'-(\lambda_0^{-4}+\tau\Omega/2)V=0\ \ (y=0)\\&\lambda_0^{-4}V'-(\lambda_0^{-4}+\tau\Omega/2)U-Q/2\pi+4\pi(\gamma/\mu\ell)V-\Omega\mathrm{cotanh}(\mathrm{y}_B)V=0\ \ (y=0)\\&U=0\ \ \ (y=-y_B)\\&V=0\ \ \ (y=-y_B)\end{aligned}\right\} \tag{SM-5}$$

If $\lambda_0=1$, the linearly independent solutions to the 4th order system (SM-4) are

$$\left.\begin{aligned}&U=-c_1e^{y}-c_2(1+y)e^{y}+c_3e^{-y}-c_4(1-y)e^{-y}\\&V=c_1e^{y}+c_2ye^{y}+c_3e^{-y}+c_4ye^{-y}\\&Q=2\pi\left(2c_2e^{y}+2c_4e^{-y}\right)\end{aligned}\right\} \tag{SM-6}$$

If $\lambda_0>1$ the solutions are

$$\left.\begin{aligned} U &= -c_1 e^{y} - c_2 \lambda_0^{\,3} e^{\lambda_0^{\,3} y} + c_3 e^{-y} + c_4 \lambda_0^{\,3} e^{-\lambda_0^{\,3} y} \\ V &= c_1 e^{y} + c_2 e^{\lambda_0^{\,3} y} + c_3 e^{-y} + c_4 e^{-\lambda_0^{\,3} y} \\ Q &= 2\pi(\lambda_0^{\,2} - \lambda_0^{\,-4})\left(-c_1 e^{y} + c_3 e^{-y}\right) \end{aligned}\right\} \qquad \text{(SM-7)}$$

Two methods to generate solutions to this eigenvalue problem are outlined below. For each method, first express c_3 and c_4 in terms of c_1 and c_2 by enforcing the boundary conditions on $y = -y_B$ in (SM-5). Then, express the two boundary conditions on $y = 0$ in (SM-5) which provides 2 linear homogeneous equations for c_1 and c_2 whose determinant is the desired condition for the eigenvalues Ω. In addition to the pre-stretch, λ_0, dimensionless surface energy, $\gamma / \mu\ell = (\gamma / \mu h)(h / \ell)$, and τ, the only parameter is the dimensionless layer thickness $y_B = 2\pi h / \ell$. The critical (lowest) eigenvalue is minimized with respect to the dimensionless mode number $h / \ell = hk / 2\pi$. Alternatively, one can evaluate $\Delta\Psi_2 / \mu\ell^2$ in (SM-3) in terms of c_1 and c_2 using numerical integration for any specified set of parameters and Ω. Considering all possible mode numbers, the critical eigenvalue is the lowest value of Ω for which $\Delta\Psi_2 / \mu\ell^2 = 0$. These two methods are readily implemented and yield results of high accuracy using standard numerical algorithms with double precision arithmetic.

It is difficult to produce closed form formulas by carrying out either of the above procedures analytically when the critical mode interacts with the bottom of the layer. However, when the critical eigenvalue lies within the short wavelength limit, exact analytic formulas for the eigenvalues and associated eigenmodes presented in Section 2 can be obtained. In the short wavelength limit $y_B = 2\pi h / \ell \to \infty$ in (SM-3) - (SM-5) with $c_3 = c_4 = 0$. The boundary conditions on $y = 0$ in (SM-5) provide the eigenvalue condition as two homogeneous equations for c_1 and c_2. These can be reduced analytically to the give the formulas for the critical eigenvalues (2.1), (2.3) and (2.4) and the associated eigenmodes (2.2) and (4.3). As a check on the validity of the analytic formulas, we have carried out the numerical procedures described in the previous paragraph and produced identical results to those generated by the formulas.

In carrying out the bifurcation analysis for other constitutive models, such as the Gent model, using the methods employed in this paper, one must derive the quadratic bifurcation

functional for the specific model. Hill's (1961) approach to bifurcation in finitely strained solid bodies, which is similar in many respects to that of Biot (1965), provides a short cut to the derivation. As noted in the text, Hill's approach was used to generate the functional for the Gent material in (4.4). In the limit $J_L \to \infty$ for the neo-Hookean material the functional (4.4) appears to be different from corresponding result derived from (4.1), but it is readily shown they are identical apart from terms that vanish due to the incompressibility constraint.

The electro-static energy changes for deformations of period ℓ

In this section, we fill in some of the omitted steps in Section 3.2 of the paper. Application of Green's theorem to (3.6), transforms it to an integral along C,

$$\Delta U_{electric} = \frac{1}{2}\varepsilon V_0'^2 \int_{-\ell/2}^{\ell/2} \left(2\varphi + \varphi\varphi_{,i} n_i\right)\sqrt{1+Y'^2}\, dx_1 , \qquad \text{(SM-8)}$$

because the contributions from the vertical sides of the section in Fig. 3 cancel each other by periodicity and the contribution along the bottom of the layer is exponentially small if $\ell << h$. Here, n_i is the unit normal to C with components $n_1 = -Y'/\sqrt{1+Y'^2}$ and $n_2 = 1/\sqrt{1+Y'^2}$ where $Y' = dY/dx_1$ (see Fig. 6 for Problem I).

The next step is to solve for the change in the potential φ as dependent on the shape change Y and to evaluate (SM-8). The stability analysis conducted in this paper requires $\Delta U_{electric}$ to be known to order Y^3, and thus we will neglect contributions of order Y^4 and smaller.

Using the fact that $\varphi = -Y$ on C, the first contribution to (SM-8) becomes

$$2\int_{-\ell/2}^{\ell/2} \varphi\sqrt{1+Y'^2}\, dx_1 = -2\int_{-\ell/2}^{\ell/2} Y(x_1)\left(\sqrt{1+Y'^2} - 1\right) dx_1 \qquad \text{(SM-9)}$$

where use has been made of the fact that $\int_{-\ell/2}^{\ell/2} Y dx_1 = 0$. Evaluation of the second contrition in (SM-8) requires determination of $\varphi(x_1, x_2)$. Using Fourier series, $\varphi(x_1, x_2) = \sum_{j=0}^{\infty} f_j(x)\cos(jkx_1)$,

with $k = 2\pi / \ell$ (consistent with symmetry about $x_1 = 0$), one finds the solution to $\nabla^2 \varphi = 0$ with $\varphi = -Y$ on C to be

$$\varphi(x_1, x_2) = \sum_{j=0}^{\infty} \varphi_j e^{jkx_2} \cos(jkx_1) \qquad \text{(SM-10)}$$

with the φ_j satisfying

$$\sum_{j=0}^{\infty} \varphi_j e^{jkY(x_1)} \cos(jkx_1) = -Y(x_1) \qquad \text{(SM-10)}$$

The integrand of the second contribution to (SM-8) is (without approximation)

$$\varphi \varphi_{,i} n_i \sqrt{1+Y'^2}\, dx_1 = -Y \left(Y' \sum_{j=1} jk\varphi_j e^{jkY} \sin jkx_1 + \sum_{j=1} jk\varphi_j e^{jkY} \cos jkx_1 \right) dx_1$$

Then, with the use of the derivative of (SM-10) with respect to x, one obtains

$$\varphi \varphi_{,i} n_i \sqrt{1+Y'^2}\, dx_1 = -Y \left(Y'^2 + \left(1+Y'^2\right) \sum_{j=1} jk\varphi_j e^{jkY} \cos jkx_1 \right) dx_1$$

Combining both contributions in (SM-8) gives (without approximation)

$$\Delta U_{electric} = -\frac{1}{2} \varepsilon V_0'^2 \left\{ \int_{-\ell/2}^{\ell/2} \left(2Y \left(\sqrt{1+Y'^2} - 1 \right) + YY'^2 \right) dx_1 + \int_{-\ell/2}^{\ell/2} \left(Y \left(1+Y'^2\right) \sum_{j=1} jk\varphi_j e^{jkY} \cos jkx_1 \right) dx_1 \right\} \qquad \text{(SM-11)}$$

Inspection of the second term above reveals we must obtain the first, $\varphi_i^{(0)}$ and second, $\varphi_i^{(1)}$, order contributions to $\varphi_i = \varphi_i^{(0)} + \varphi_i^{(1)}$ if the energy change is to be evaluate to order Y^3.

To lowest order, for sufficiently small Y, the solution to (SM-10) is

$$\varphi_j \equiv \varphi_j^{(0)} = -\frac{2}{\ell} \int_{-\ell/2}^{\ell/2} Y(x_1) \cos jk dx_1 = -Y_j \quad \text{where } Y(x_1) = \sum_{j=1}^{\infty} Y_j \cos jkx_1 \qquad \text{(SM-12)}$$

Note that $\varphi_0^{(0)} = Y_0 = 0$ because $\int_{-\ell/2}^{\ell/2} Y dx_1 = 0$. Using the expansion, $e^{jkY(x_1)} = 1 + jkY(x_1) + O(Y^2)$ in (SM-10), one obtains

$$\sum_{j=0}^{\infty} \varphi_j^{(1)} \cos jkx_1 = \sum_{j=1}^{\infty} jkY_j Y(x_1) \cos jkx_1 \qquad \text{(SM-13)}$$

The solution of (SM13) is

$$\varphi_m^{(1)} = \frac{k}{2} \sum_{j=1}^{\infty} \sum_{n=1}^{\infty} j\left(\beta(m, j+n) + \beta(n, j+m) + \beta(j, m+n)\right) Y_j Y_n \qquad \text{(SM-14)}$$

where, for any integers i and j, $\beta(i, j) = 1$ if $i = j$ and $\beta(i, j) = 0$ if $i \neq j$. The error in using $\varphi_i^{(0)} + \varphi_i^{(1)}$ as an approximation to φ_i is of order Y^3.

To evaluate the energy change to order Y^3, make use of $\varphi_i = \varphi_i^{(0)} + \varphi_i^{(1)}$ in (2.7), deleting terms of order Y^4 and smaller. For completeness, the intermediate steps are presented:

$$\Delta U_{electric} = -\frac{1}{2} \varepsilon V_0'^2 \left\{ \int_{-\ell/2}^{\ell/2} \left(2Y\left(\sqrt{1+Y'^2} - 1\right) + YY'^2 \right) dx_1 + \int_{-\ell/2}^{\ell/2} \left(Y\left(1+Y'^2\right) \sum_{j=1} jk\varphi_j e^{jkY} \cos jkx_1 \right) dx_1 \right\}$$

$$\Delta U_{electric} = -\frac{1}{2} \varepsilon V_0'^2 \left\{ \int_{-\ell/2}^{\ell/2} 2YY'^2 dx_1 + \int_{-\ell/2}^{\ell/2} \left(\left(Y + YY'^2\right) \sum_{m=1} mk(-Y_m + \varphi_m^{(1)})(1 + mkY) \cos mkx_1 \right) dx_1 \right\}$$

$$\Delta U_{electric} = -\frac{1}{2} \varepsilon V_0'^2 \left\{ -\frac{\ell k}{2} \sum_{m=1} mY_m^{\,2} + \int_{-\ell/2}^{\ell/2} 2YY'^2 dx_1 - \sum_{m=1} (mk)^2 Y_m \int_{-\ell/2}^{\ell/2} Y^2 \cos mkx_1 dx_1 + \sum_{m=1} mk\varphi_m^{(1)} \int_{-\ell/2}^{\ell/2} Y \cos mkx_1 dx_1 \right\}$$

Because, $\int_{-\ell/2}^{\ell/2} Y^2 \cos mkx_1 dx_1 = \frac{\ell}{4} \sum_j \sum_n Y_j Y_n \left(\beta(m, j+n) + \beta(j, m+n) + \beta(n, j+m)\right)$ it follows that

$$-\sum_m (mk)^2 Y_m \int_{-\ell/2}^{\ell/2} Y^2 \cos mkx_1 dx_1 = -\frac{\ell k^2}{4} \sum_m \sum_j \sum_n m^2 \left(\beta(m, j+n) + \beta(j, m+n) + \beta(n, j+m)\right) Y_m Y_j Y_n$$

and,

$$\sum_{m=1} mk\varphi_m^{(1)} \int_{-\ell/2}^{\ell/2} Y \cos mkx_1 dx_1 = \frac{\ell k^2}{4} \sum_m \sum_j \sum_n Y_m Y_j Y_n mj \left(\beta(m, j+n) + \beta(n, j+m) + \beta(j, m+n)\right)$$

and,

$$\int_{-\ell/2}^{\ell/2} 2YY'^2 dx_1 = 2k^2 \sum_m \sum_j \sum_n jnY_m Y_j Y_n \int_{-\ell/2}^{\ell/2} \cos mkx \sin jkx \sin nkx dx$$
$$= \frac{\ell k^2}{2} \sum_m \sum_j \sum_n jnY_m Y_j Y_n \left(\beta(n, j+m) + \beta(j, m+n) - \beta(m, j+n)\right)$$

The sum of terms up to and including Y^3 is the result (3.8) in the paper.

If the same procedure if followed for Problem II accounting for the fact that C is the boundary at the bottom of the periodic sector between the two electrodes (see Fig. 6), one finds the same result as (3.8) but with the sign change for the cubic terms as accounted for by τ in subsequent formulas. The derivation of (3.12) entails some of the details presented above and is more straightforward.

The initial post-bifurcation expansion including the effect of small imperfections

As discussed in Section 4.2, the analysis addresses a system with N linearly independent modes all of which have the same critical eigenvalue, Ω_C. The abstract notation introduced in Section 4.2 is used here and we pick up the development assuming Equations (4.5) - (4.10) and considering at first that no imperfections are present.

If one substitutes the expansion (4.5) into $\Delta\Psi$ in (4.6), making use of the various relations in (4.7) - (4.10), one obtains

$$\Delta\Psi = \left(\Omega_C - \Omega\right) \sum_{i=1}^{N} \xi^{(i)2} G_2(u^{(i)}) + F_3\left(\sum_{i=1}^{N} \xi^{(i)} u^{(i)}\right) - \Omega G_3\left(\sum_{i=1}^{N} \xi^{(i)} u^{(i)}\right)$$
$$+ 2\sum_{i=1}^{N} \xi^{(i)} \left(F_{11}(u^{(i)}, \Delta u) - \Omega G_{11}(u^{(i)}, \Delta u)\right) + F_2(\Delta u) - \Omega G_2(\Delta u) + ... \qquad \text{(SM-15)}$$

The first two term on the second line vanish by orthogonality, while the last two are of order ξ^4 and will be neglected. Rendering $\Delta\Psi$ stationary with respect to the mode amplitudes will generate set of equations relating Ω to the mode amplitudes ξ of the form $\Omega = \Omega_C + O(\xi)$.

Thus, to evaluate $\Delta\Psi$ to order ξ^3, the term ΩG_3 in (SM-15)) can be replaced by $\Omega_C G_3$. With this replacement and retaining all terms to order ξ^3, (SM-15) can be rewritten as

$$\Delta\Psi = \left(\Omega_C - \Omega\right)\sum_{i=1}^{N}\xi^{(i)2}G_2(u^{(i)}) + F_3\left(\sum_{i=1}^{N}\xi^{(i)}u^{(i)}\right) - \Omega_C G_3\left(\sum_{i=1}^{N}\xi^{(i)}u^{(i)}\right) \qquad \text{(SM-16)}$$

This can also be written as

$$\Delta\Psi = \left(1-\Omega/\Omega_C\right)\sum_{i=1}^{N}c_i\xi^{(i)2} + \sum_{j=1}^{N}\sum_{m=1}^{N}\sum_{n=1}^{N}c_{jmn}\xi^{(j)}\xi^{(m)}\xi^{(n)} \qquad \text{(SM-17)}$$

where $c_i = \Omega_C G_2(u^{(i)})$ and the coefficients in the cubic term can be evaluated in terms of the eigenmodes using the cubic contributions in (SM-16) without the need for solving for higher order terms. Stationarity of $\Delta\Psi$ with respect to each of the mode amplitudes generates the set of initial post-bifurcation equilibrium equations:

$$\left(1-\Omega/\Omega_C\right)c_i\xi^{(i)} + \sum_{j=m}^{N}\sum_{n=1}^{N}a_{imn}\xi^{(m)}\xi^{(n)} = 0,\ \ i=1,N \quad \text{with } a_{imn}=(c_{imn}+c_{min}+c_{mni})/2 \qquad \text{(SM-18)}$$

Geometric imperfections in shape of surface modes:

The reader is referred to Cao and Hutchinson (2012) for a systematic derivation of the modification of the energy functional that accounts for an initial stress-free surface undulation of the type considered here when there is no pre-stretch. The imperfection from (4.13) is

$$\overline{u}_2(x_1,0) = \ell\sum_{i=1}^{N}\overline{\xi}_i^{G}\cos(2\pi i x_1/\ell) \qquad \text{(SM-19)}$$

In the absence of pre-stretch, the lowest order contribution to the terms in the energy functional $\Delta\Psi$ that are independent of Ω are of order $\xi^2\overline{\xi}$ which are neglected compared to the contributions from the terms in $\Delta\Psi$ which are linear in Ω and quadratic in u. These are of order $\xi\overline{\xi}$. The lowest order contributions can obtained directly using terms quadratic in u and linear in Ω in either (4.1) or (4.4) by substituting $u_2 = \sum_{j=1}^{N}(\xi_j + \overline{\xi}_j)u_2^{(j)}$ into these expressions.

The terms quadratic in $\overline{\xi}$ can be ignored because they do not contribute to the variational equation. The lowest order imperfections terms are those of form $\Omega\xi\overline{\xi}$. Alternatively, substitute u_2 into $-\Omega G_2(u)$ in (4.16), disregarding $-\Omega G_2(\overline{u})$ which does not contribute to the variational equations, to obtain the additional term in (4.16):

$$-2\Omega\sum_{i=1}^{N}\xi_i G_{11}(u^{(i)},\overline{u}) = -2\mu\ell^2 C\,(\Omega/\Omega_C)\sum_{i=1}^{N} i\xi_i\overline{\xi}_i^{G} \qquad \text{(SM-20)}$$

Perturbing surface force imperfections:

Identifying the contribution of the perturbing force/area distribution introduced in (4.15) to the energy functional $\Delta\Psi$ is more straightforward than that for geometric imperfections. The perturbing force/area distribution on the top surface of the layer, $p(x_1)$, is regarded as prescribed. Thus, its potential energy contribution to the periodic sector under consideration is $-\int_{-\ell/2}^{\ell/2} p(x_1)u_2(x_1,0)dx_1$, leading to the lowest order contribution (4.16).